A Hankel Matrix Based Reduced Order Model for Stability Analysis of Hybrid Power System Using PSO-GSA Optimized Cascade PI-PD Controller for Automatic Load Frequency Control

Veerasamy, Veerapandiyan; Wahab, Noor Izzri Abdul; Ramachandran, Rajeswari; Othman, Mohammad Lutfi; Hizam, Hashim; Irudayaraj, Andrew Xavier Raj; Guerrero, Josep M.; Kumar, Jeevitha Satheesh

Published in:
IEEE Access

DOI (link to publication from Publisher):
10.1109/ACCESS.2020.2987387

Publication date:
2020

Document Version
Publisher's PDF, also known as Version of record

IEEE Access
Multidisciplinary | Rapid Review | Open Access Journal

Received April 2, 2020, accepted April 7, 2020, date of publication April 13, 2020, date of current version April 29, 2020.

Digital Object Identifier 10.1109/ACCESS.2020.2987387

A Hankel Matrix Based Reduced Order Model for Stability Analysis of Hybrid Power System Using PSO-GSA Optimized Cascade PI-PD Controller for Automatic Load Frequency Control

VEERAPANDIYAN VEERASAMY[1], (Graduate Student Member, IEEE), NOOR IZZRI ABDUL WAHAB[1], (Senior Member, IEEE), RAJESWARI RAMACHANDRAN[2], (Member, IEEE), MOHAMMAD LUTFI OTHMAN[1], (Senior Member, IEEE), HASHIM HIZAM[1], (Member, IEEE), ANDREW XAVIER RAJ IRUDAYARAJ[1], (Graduate Student Member, IEEE), JOSEP M. GUERRERO[3], (Fellow, IEEE), AND JEEVITHA SATHEESH KUMAR[2]

[1]Center for Advanced Lightning Power and Energy Research (ALPER), Department of Electrical and Electronics Engineering, University Putra Malaysia (UPM), Seri Kembangan 43400, Malaysia
[2]Department of Electrical and Electronics Engineering, Government College of Technology, Coimbatore 641013, India
[3]Center for Research on Microgrids (CROM), Department of Energy Technology, Aalborg University, 9220 Aalborg, Denmark

Corresponding authors: Veerapandiyan Veerasamy (veerapandian220@gmail.com) and Noor Izzri Abdul Wahab (izzri@upm.edu.my)

This work was funded and supported in part by Geran Putra Berimpak -University Putra Malaysia (GPB-UPM) grant under Grant no. 9630000, and in part by VILLUM FONDEN under the VILLUM Investigator Grant (no. 25920): Center for Research on Microgrids (CROM), in the recently accepted manuscript "A hankel matrix based reduced order. Model for stability analysis of hybrid power system using PSO-GSA optimized Cascade PI-PD controller for Automatic Load Frequency Control."

ABSTRACT This paper presents the automatic load frequency control (ALFC) of two-area multisource hybrid power system (HPS). The interconnected HPS model consists of conventional and renewable energy sources operating in disparate combinations to balance the generation and load demand of the system. In the proffered work, the stability analysis of nonlinear dynamic HPS model was analyzed using the Hankel method of model order reduction. Also, an attempt was made to apply cascade proportional integral – proportional derivative (PI-PD) control for HPS. The gains of the controller were optimized by minimizing the integral absolute error (IAE) of area control error using particle swarm optimization–gravitational search algorithm (PSO-GSA) optimization technique. The performance of cascade control was compared with other classical controllers and the efficiency of this approach was studied for various cases of HPS model. The result shows that the cascade control produced better transient and steady state performances than those of the other classical controllers. The robustness analysis also reveals that the system overshoots/undershoots in frequency response pertaining to random change in wind power generation and load perturbations were significantly reduced by the proposed cascade control. In addition, the sensitivity analysis of the system was performed, with the variation in step load perturbation (SLP) of 1% to 5%, system loading and inertia of the system by ±25% of nominal values to prove the efficiency of the controller. Furthermore, to prove the efficiency of PSO-GSA tuned cascade control, the results were compared with other artificial intelligence (AI) methods presented in the literature. Further, the stability of the system was analyzed in frequency domain for different operating cases.

INDEX TERMS Automatic load frequency control (ALFC), hybrid power system (HPS), cascade control scheme (CCs), proportional integral – proportional derivative (PI-PD) control, Hankel method, particle swarm optimization – gravitational search algorithm (PSO-GSA).

I. INTRODUCTION

Nowadays, the interconnected power system is more complex and stressed due to the increasing size of the grid. Moreover, the restructuring of system with emerging

The associate editor coordinating the review of this manuscript and approving it for publication was Derek Abbott.

renewable energy (RE) sources, uncertainties in system parameters or load, and environmental condition increase the frequency and tie-line power fluctuations of the system. Therefore, automatic generation control (AGC) or automatic load frequency control (ALFC) plays a significant role to maintain the generation–load balance under serious disturbances for secure and reliable system operation by controlling the frequency and tie-line power oscillation. Recently, the increased penetration level of intermittent nature of RE sources into the grid increases the uncertainty of power system assets and control operation, leading to the blackout of the system [1]–[3]. Therefore, it is necessary to provide an effective robust control strategy to accomplish a trade-off between system security, efficiency, and reliability under unfavorable conditions. Over the years, researchers have proposed numerous classical and robust control strategies to maintain the stability of system for ALFC application. However, the rapid growth of power system requires quicker solution, i.e., controller with faster steady state, transient performance, and high degree of reliability. In addition, the type and design of controller are the major factors which influence the performance and stability of the system remarkably.

Robust controller schemes such as sliding mode control (SMC) and second-order SMC, distributed model predictive control, $H_2/H\infty$ and model free control strategy are used for ALFC applications [4]–[8]. However, these methods are difficult to implement in real time as it involves complex mathematics in deriving the control law. Most of the recently published research works in this area ignored system uncertainties and practical constraints, and recommended complex control structures with unrealistic frameworks that may have few difficulties in real-time applications. At present, the utilities use simple classical integral (I), proportional integral (PI), proportional derivative (PD), proportional integral derivative (PID), tilt integral derivative [9] and integral minus proportional derivative (IPD) [10] controllers than the complex control strategy portrayed in the literature for real-time ALFC applications. However, setting the gain values of these classical controllers is a cumbersome process for industrial applications that involve nonlinearities, higher order system, and delay time. In the last few decades, the gain values of the controller are tuned based on experience through trial and error approach and classical tuning methods like Ziegler and Nichols [11]. However, their performance is incapable for wide range of operating conditions and random load variations [12], [13]. Besides, AI techniques such as neural network (NN), fuzzy logic system (FLS), and neuro-fuzzy system are widely used to tune the parameters of controller [14]–[19]. However, the NN requires proper training of the network and longer convergence time. On the contrary, the FLS depends on field expertise in tuning the membership functions [13]. Therefore, the gain values of classical controllers are usually obtained by heuristic methods like genetic algorithm (GA), particle swarm optimization (PSO), grasshopper optimization algorithm (GOA), salp swarm algorithm (SSA), selfish herd optimization (SHO), and quasi–oppositional selfish herd optimization (QSHO) for a trade-off between efficacy and robustness [20]–[27]. However, these methods are proposed for single loop control strategy of ALFC application.

The cascade control scheme (CCs) introduced by Franks and Worley gives superior performance than the simple single loop control system, particularly in the presence of disturbances. Among the various combinations of cascade controller terms, the PI-PD gives the best disturbance rejection performance [28]–[30]. The CCs is widely used in process control and DC-DC converter control applications, its needs and benefits are discussed in [29]. Recently, Puja Dash et.al and Gheisarnejad et.al used the cascade PI-PID and PI-PD control strategies for ALFC application of multi-area system using flower pollination optimization algorithm (FPA) and improved jaya algorithm, respectively. The study reveals that the cascade PI-PD controller performed better than the I, PI, PID, and cascade PI-PID controllers [31], [32]. Later, Padhy and Panda [33], also investigated the cascade PI-PD controller using hybrid stochastic fractal and pattern search technique for ALFC application in the presence of thermal, hydro and gas power plant with presence of electric vehicle. The moth flame optimization (MFO) and improved grey wolf optimization (IGWO) based cascade controllers were also presented in [34], [35]. Similar approach was also used in the process control application, and the authors claimed that as the number of tuning knobs increases, the controller's performance may improve [36], [37]. However, the efficiency of cascade control in HPS model is not studied, and the stability of the system model was unable to be analyzed in the literature. Therefore, this paper aims to apply the CCs for HPS model to regulate the frequency and tie-line power fluctuations, as well as to study the stability of the system through the model order reduction techniques.

In this study, the HPS model involves multisource power generation like thermal, hydro, gas, and RE sources such as wind and diesel power generation. The integrated HPS also consists of energy storage system like aqua electrolyzer (AE), fuel cell (FC), and battery storage system (BESS) to restore the stability of system due to the intermittent nature of wind power generation. Thus, the inner loop of CCs responds to the dynamics initiated by the generation sources and the controller in the outer loop handles the power system dynamics and load perturbations. Therefore, the performance of cascade control is more effective than that of the conventional feedback control [38]. Furthermore, the stability of the system is another major concern of the utilities. The authors in [26] presented an eigen value analysis to analyze the stability of the system. However, these techniques involve mathematical calculation and the complexity increases in large size systems. In addition, it increases the dynamics associated with the system that leads to many numbers of state variables to be controlled. To cater such limitations, this paper proposes the model order reduction approach to analyze the stability of the system using frequency response analysis.

To achieve the aforementioned objectives, the PSO-GSA based hybrid optimization technique by combining the non-swarm intelligence based GSA algorithm and swarm intelligence based PSO algorithm was used. The PSO-GSA improves the search and convergence ability of the method by deriving the advantages of collective behavior of swarm and attractive forces of particle in nature of physics. Thus, it possesses the characteristics of exploration and exploitation. Hence, it enhances the efficacy in obtaining the global optimal solution [39]–[42]. The application of PSO-GSA based optimization is also proved to be efficient for frequency control, voltage regulation, and stability assessment [43]–[45]. Therefore, a hybrid PSO-GSA based technique was used to tune the gains of controller for ALFC application of two-area interconnected HPS in this proposed work. Furthermore, the sensitivity analysis of the controller was carried out based on the variation of step load change, inertia of the machine, and loading of the system to select the best controllers for the dynamic operation of system [26], [31]. Surprisingly, no literature work has dealt with CCs for multisource multi-area HPS and it is difficult to predict which CCs combination performs better. This motivates the authors to investigate the best suited combination of CCs for HPS operation. The CCs speeds up the response of the system by improving the settling time and overshoot unlike the single controller. Therefore, to reduce the steady state error in the output of the system and computational complexity involved in the design of proposing controller, the integral absolute error (IAE) index was chosen as the objective function for tuning the gain parameters of the controller. In view of the above literature study, the main contributions of this paper are as follows:

(a) To optimize gains of various classical controllers such as I, PI, PID, IPD and other combination of cascade controllers like PI-PD, I-PD, P-PD and PD-PI for various combination of multi-source power system using PSO-GSA method.
(b) To compare the transient and steady state performance indices of dynamic responses with various controllers and to find the best controller with minimum control effort.
(c) Analysis of the dynamic responses among, I, PI, IPD, PID and the best optimal cascade controller when the system undergoes random load and wind power variations simultaneously.
(d) To test the robustness of the best proven controller under wide variations in system loading, inertia constant and step load perturbation (SLP) with control parameters obtained at nominal loading using sensitivity analysis.
(e) Derivation of the state space model of HPS was considered and the reduced order matrix was obtained in Hankel form to analyze the stability of the best optimal controller found in (b).

This paper is organized as follows: Section 2 describes the hybrid system model studied with state space modeling of the system. Sections 3 and 4 elucidate the cascade control scheme and computational intelligence (CI) based PSO-GSA method to tune the gain values of the controller. Results and discussion of system model under various case of operation is illustrated in Section 5. Section 6 portrays the comparison of the best CCs with other cascade controllers and the control techniques proposed in recent literature work. Section 7 and 8 explains the stability analysis using Hankel form of model order reduction and the outcome of this study, respectively. Future scope of the work is also presented in last part of the paper.

II. SYSTEM MODEL

The HPS considered in this study consists of reheat thermal, hydro, gas, wind power, diesel, AE, FC, and BESS as depicted in Figure 1. The parameters used for the simulation are given in Appendix.

A. MODEL OF WIND ENERGY CONVERSION SYSTEM (WECS)

The wind energy conversion system (WECS) is the first RE source to be installed in large scale compared to other RE sources. The output of wind turbine generator (WTG) depends on the instantaneous speed of wind flow. The detailed characteristics and modeling of WECS are portrayed in [46]. Though the WECS is associated with several nonlinearities, the pitch control in wind turbine will prevent the power fluctuations. For small disturbance, the system nonlinearity was linearized with few approximations and the linearized transfer function can be considered and expressed as [20], [46]:

$$G_{\mathrm{WTG}}(s) = \frac{K_{\mathrm{WTG}}}{1 + sT_{\mathrm{WTG}}} \tag{1}$$

where K_{WTG} and T_{WTG} are the gain and time constant of WTG, respectively.

B. MODEL OF DIESEL ENERGY GENERATOR

The diesel energy generator (DEG) provides the driving torque for synchronous generator of the system. The dynamic response of DEG makes it to supply power for the peak load demand during sudden increase in the load demand. The DEG maintains the system frequency when no or less wind blows into WECS that leads to no or intermittent generation. To preserve stable system operation, it is required to operate a diesel generator in line with WECS and adjust the loading pattern during the variation of wind power. Therefore, a DEG was considered and modeled with the WECS system. The DEG is a nonlinear system due to the presence of nonlinearities such as time variant dead time between fuel injection and generation of mechanical torque. Hence, the DEG was modeled by a single order transfer function as [20], [46]:

$$G_{\mathrm{DEG}}(s) = \frac{K_{\mathrm{DEG}}}{1 + sT_{\mathrm{DEG}}} \tag{2}$$

where K_{DEG} and T_{DEG} are the gain and time constant of DEG, respectively.

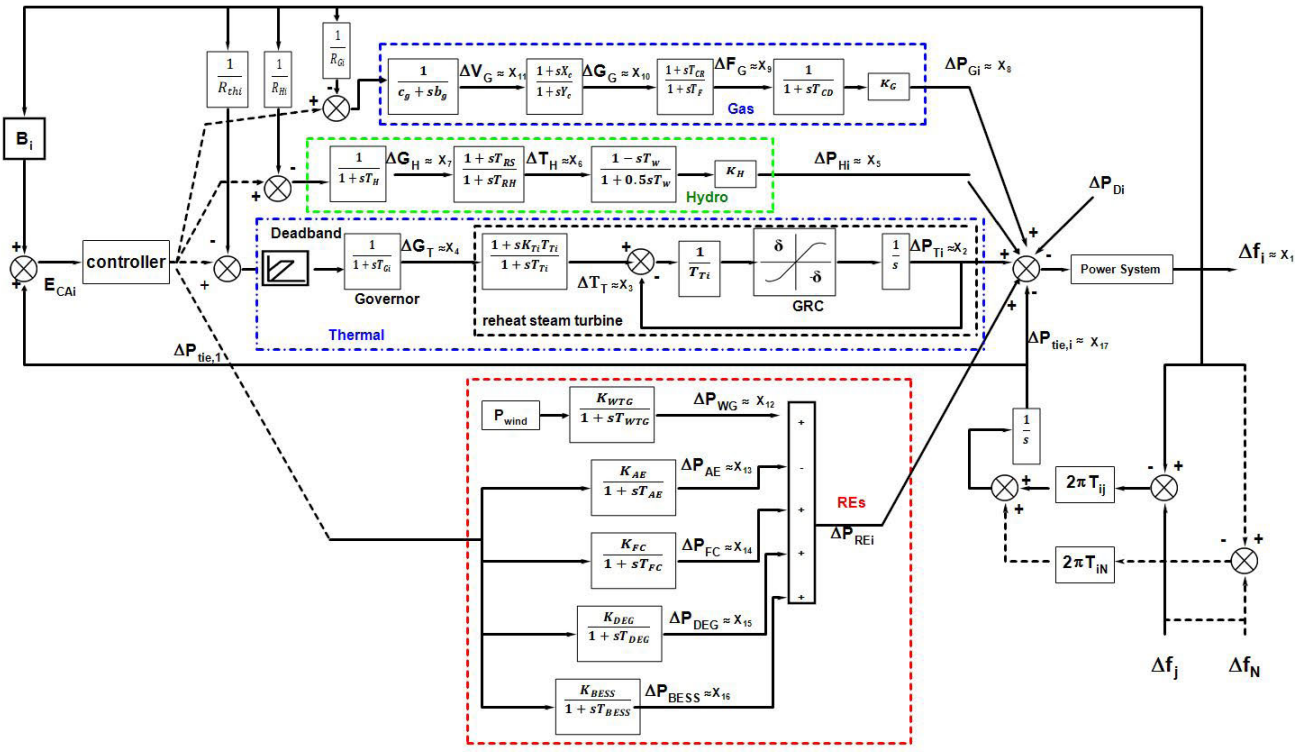

FIGURE 1. Block diagram of multi-units HPS model.

C. MODEL OF AE AND FC

The combination of AE and FC is majorly used with the grid-connected or standalone distributed energy sources like wind power generation, solar photovoltaic, and energy storage system. In this work, a WECS and DEG based RE sources were considered for ALFC application. The rapid fluctuations in the output power of WECS are absorbed by the AE and the hydrogen generated used as fuel for FC. The hydrogen is used to generate the power from FC, which reduces the power oscillation in the grid. The precise model of AE-FC involves high-order model with nonlinearities that include power conditioner and controller. For a large scale interconnected power system, the first-order transfer function can be considered without compromising their exact representation of the AE-FC model and expressed as below [20], [46]:

$$G_{\mathrm{FC}}(s) = \frac{K_{\mathrm{FC}}}{1 + sT_{\mathrm{FC}}} \tag{3}$$

$$G_{\mathrm{AE}}(s) = \frac{K_{\mathrm{AE}}}{1 + sT_{\mathrm{AE}}} \tag{4}$$

where K_{FC} and K_{AE} are the gain constant, T_{FC} and T_{AE} are the time constant of FC and AE, respectively.

D. MODEL OF BATTERY ENERGY STORAGE SYSTEM

The intermittent nature of WECS causes continuous power fluctuations in the grid and results in instability of the system. The probable solution is to store the excess electrical energy generated from WECS in the battery. The BESS can supply large amount of power for longer period provided with a huge battery bank connected to the utility grid. By linearizing the nonlinearities associated with the system, the simplified transfer function model for small-signal analysis is taken as [20], [46]:

$$G_{\mathrm{BESS}}(s) = \frac{K_{\mathrm{BESS}}}{1 + sT_{\mathrm{BESS}}} \tag{5}$$

where K_{BESS} and T_{BESS} are the gain and time constant of BESS, respectively.

E. STATE SPACE MODEL OF HPS

The dynamics associated with the system are represented by the set of first-order differential equations using state variables called state equations or state-space model [28]. The state-space analysis governing the HPS model presented in Figure 1 is performed in the absence of secondary control actions of ALFC loop. Also, the analysis is shown for the general i^{th} area power system model considering the change in load disturbances ΔP_{Di} and speed position ΔP_{ci} for analysis [26]. The total number of state variables used to model the HPS will be 17 and its vector form is given as follows:

$$X = [X_1, X_2, X_3, \ldots, X_{17}]^T \tag{6}$$

The state variables associated with the system parameters are represented as:

$$X = [\Delta f_i \ \Delta X_{1T} \ \Delta X_{1H} \ \Delta X_{1G} \ \Delta X_{1\mathrm{RE}} \ \Delta P_{\mathrm{tie},i}]^T \tag{7}$$

where,

$$\Delta X_{1T} = [\Delta P_T \ \Delta T_T \ \Delta G_T] \tag{8}$$

$$\Delta X_{1H} = [\Delta P_H \ \Delta T_H \ \Delta G_H] \quad (9)$$
$$\Delta X_{1G} = [\Delta P_G \ \Delta F_G \ \Delta G_G \ \Delta V_G] \quad (10)$$
$$\Delta X_{1\text{RE}} = [\Delta P_{\text{WG}} \ \Delta P_{\text{AE}} \ \Delta P_{\text{FC}} \ \Delta P_{\text{DEG}} \ \Delta P_{\text{BESS}}] \quad (11)$$

The state-space equations corresponding to HPS are detailed as follows:

$$\dot{X}_1 = \frac{K_{pi}}{T_{pi}}[-X_1 + X_8 + X_5 + X_2 - X_{14} + X_{12} - \Delta P_{Di}] \quad (12)$$

The state-space modeling for thermal system is as follows:

$$\dot{X}_2 = \frac{-X_2}{T_{ti}} + \frac{X_3}{T_{ti}} \quad (13)$$
$$\dot{X}_3 = -\frac{X_3}{T_{ri}} + [\frac{1}{T_{ri}} - \frac{k_r}{T_{Gi}}]X_4 + \frac{1}{T_{ri}}\Delta P_{ci} - \frac{X_1}{T_{ri}R_{\text{th}i}} \quad (14)$$
$$\dot{X}_4 = \frac{-X_4}{T_{Gi}} + \frac{\Delta P_{ci}}{T_{Gi}} - \frac{1}{R_{\text{th}i}T_{Gi}}X_1 \quad (15)$$

The state-space modeling for hydro system is depicted as:

$$\dot{X}_5 = -a_1X_5 + [a_1 - a_2]X_6 - a_2(1-\frac{T_{\text{rs}}}{T_{\text{gh}}}) + X_7 - a_3\Delta P_{ci} - \frac{a_3}{R_{Hi}}X_1 \quad (16)$$

where

$$a_1 = \frac{2K_H}{T_w}, \quad a_2 = \frac{2K_H}{T_{\text{rh}}}, \ a_3 = \frac{2K_HT_{\text{rs}}}{T_{\text{gh}}T_{\text{rh}}}$$
$$\dot{X}_6 = \frac{-X_6}{T_{\text{rh}}} + a_4X_7 + a_5\Delta P_{ci} - \frac{a_5}{R_{Hi}}X_1 \quad (17)$$

where

$$a_4 = [\frac{1}{T_{\text{rh}}} - \frac{T_{\text{rs}}}{T_{\text{gh}}}], \quad a_5 = \frac{T_{\text{rs}}}{T_{\text{rh}}T_{\text{gh}}}$$
$$\dot{X}_7 = \frac{-X_7}{T_{\text{gh}}} + \frac{1}{T_{\text{gh}}}\Delta P_{ci} - \frac{X_1}{T_{\text{gh}} - R_{Hi}} \quad (18)$$

The state-space modeling for gas power generation system is represented as:

$$\dot{X}_8 = \frac{-K_G}{T_{\text{cd}}}X_8 + \frac{K_G}{T_{\text{cd}}}X_9 \quad (19)$$
$$\dot{X}_9 = \frac{-X_9}{T_{\text{fc}}} + X_{10}[\frac{1}{T_{fc}} - a_7] + X_{11}[a_7 - a_6c_g] + a_6\Delta P_{ci} - \frac{a_6}{R_{Gi}}X_1 \quad (20)$$

where

$$a_6 = \frac{x_cT_{\text{cr}}}{y_cb_gT_{\text{fc}}}, \quad a_7 = \frac{T_{\text{cr}}}{T_{\text{fc}}y_c}$$
$$\dot{X}_{10} = \frac{-X_{10}}{y_c} + X_{11}[\frac{1}{y_c} - a_8c_g] + a_8\Delta P_{ci} - \frac{a_8}{R_{Gi}}X_1 \quad (21)$$

where

$$a_8 = \frac{x_c}{y_cb_g}$$
$$\dot{X}_{11} = \frac{-c_g}{b_g}X_{11} + \frac{1}{b_g}\Delta P_{ci} - \frac{X_1}{b_g - R_{Gi}} \quad (22)$$

The state-space equation for RE sources is modeled as follows:

$$\dot{X}_{12} = -\frac{X_{12}}{T_{\text{WTG}}} + K_{\text{WTG}}P_{\text{Wind}} \quad (23)$$
$$\dot{X}_{13} = \frac{-X_{13}}{T_{\text{AE}}} + \frac{K_{\text{AE}}}{T_{\text{AE}}}\Delta P_{ci} \quad (24)$$
$$\dot{X}_{14} = \frac{-X_{14}}{T_{\text{DEG}}} + \frac{K_{\text{DEG}}}{T_{\text{DEG}}}\Delta P_{ci} \quad (25)$$
$$\dot{X}_{15} = \frac{-X_{15}}{T_{\text{FC}}} + \frac{K_{\text{FC}}}{T_{\text{FC}}}\Delta P_{ci} \quad (26)$$
$$\dot{X}_{16} = \frac{-X_{16}}{T_{\text{BESS}}} + \frac{K_{\text{BESS}}}{T_{\text{BESS}}}\Delta P_{ci} \quad (27)$$

The interconnected tie-lines of i^{th} area power system is portrayed as follows:

$$\dot{X}_{17} = \Delta P_{\text{tie},i} = 2\pi\left[\sum_{i=1,\, i\neq j}^{n} T_{ij}X_i\right] \quad (28)$$

From the above analysis, the state matrix A, input matrix B and the output matrix C can be obtained. The general state-space equation of the system is defined as,

$$\dot{X} = AX + Bu \quad (29)$$

where u is the control input and is expressed as:

$$u = [\Delta P_{ci}]^T \quad (30)$$

The output matrix of the system is defined as:

$$Y = CX \quad (31)$$

The output state vector of the system is as follows:

$$Y = [\ \Delta f_i \ \Delta P_{\text{TH}} \ \Delta P_H \ \Delta P_G \ \Delta P_{\text{RE}} \ \Delta P_g \ ]^T \quad (32)$$
$$\Delta P_{\text{RE}} = \Delta P_{\text{WG}} - \Delta P_{\text{AE}} + \Delta P_{\text{FC}} + \Delta P_{\text{DEG}} + \Delta P_{\text{BESS}} \quad (33)$$
$$\Delta P_g = \Delta P_{\text{TH}} + \Delta P_H + \Delta P_G + \Delta P_{\text{RE}} \quad (34)$$

The above state-space modeling is derived for i^{th} area of HPS in generalized form, the modeling of various cases of HPS can be obtained from this analysis. Thus, the operation of thermal source in both the areas of case 1 resulting in 13 state variables, case 2 consists of multi-source power system such as thermal, hydro and gas in both the areas that result in 31 state variables, case 3 consists of thermal and RES in both area 1 and area 2 that resulting in 27 state variables. Similarly, case 4 consists of thermal, hydro and gas operation in area 1, thermal and RES in area 2 resulting in 31 state variables.

III. CASCADE CONTROL SCHEME

Cascaded control techniques evolved from the concept of sequential processes where the output of inner loop is the input to the outer loop of the system in sequence as given in Figure 2. The measurement variable exists in both the inner and outer loops of the system. The main features of cascaded controllers are given below [28]–[30], [47],

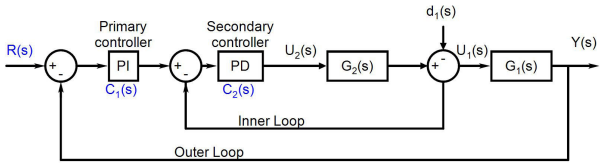

FIGURE 2. Closed loop cascade control system.

(a) The inner measurement is to suppress the effect of disturbances supplied on the outer process in the sequence.
(b) The outer process measurement is to control the quality of final output of the system.

The cascade control is mostly used to attain rapid rejection of disturbance before it spread to other parts of the plant. The outer and inner loop of CCs are explained in the following sections.

A. OUTER LOOP

The outer loop is the primary or main loop of the system, which contains the process or plant under control. The outer plant is defined as $G_1(s)$. The output of the complete cascade controller is:

$$Y(s) = G_1(s) + G_2(s) \tag{35}$$

where $U_1(s)$ is the input of outer loop and is equivalent to the output of inner loop $Y_2(s)$ and so,

$$U_1(s) = Y_2(s) \tag{36}$$

Thus, the overall objective of the outer control loop is to make the output to track the reference $R(s)$ in the presence of load disturbance $d_1(s)$. Among the various term of K_p, K_i and K_d, the proposed work used the PI term in the outer loop for load disturbance rejection and better reference tracking.

B. INNER LOOP

The inner loop is also called the slave or secondary loop and consists of multi-source generating source as $G_2(s)$ and the entire process is subjected to load perturbation of $d_1(s)$. The inner process equation is given by:

$$Y_2(s) = G_2(s)U_2(s) + d_1(s) \tag{37}$$

It comprises inner loop measurement $Y_2(s)$, which is perturbed by the system uncertainties. The main aim of the inner loop is to attenuate the effect of system modeling and limit the inner process gain variation on the control system performance. Among the three terms, the inner loop requires a fast supply disturbance rejection with high gain PD term in the inner loop. The closed loop control of interconnected plant with cascaded PI-PD controller is shown in Figure 2.

C. PI-PD CASCADED CONTROLLER

The system was modeled as a single loop control system with a PID controller and a cascade loop with PI-PD controller. The performance of reference tracking and disturbance rejection was compared for both control system responses. The transfer function of cascade control system with inner PD and outer PI controller are represented as $C_2(s)$ and $C_1(s)$, respectively.

$$C_1(s) = K_P + \frac{K_i}{s} \tag{38}$$

$$C_2(s) = K_P + K_d s \tag{39}$$

The general performance of cascade system can be studied by using the closed loop transfer function (CLTF) as given in (42)

$$Y_{11}(s) = \left[\frac{G_1(s)G_2(s)C_1(s)C_2(s)}{W(s)}\right]R(s) \tag{40}$$

$$Y_{12}(s) = \left[\frac{G_1(s)}{W(s)}\right]d_1(s) \tag{41}$$

where

$$W(s) = 1 + G_2(s)C_2(s) + G_1(s)G_2(s)C_1(s)C_2(s)]$$
$$Y(s) = Y_{11}(s) - Y_{12}(s) \tag{42}$$

where $G_1(s)$ is the main control loop; $G_2(s)$ is the slave control loop and $d_1(s)$ is the load perturbation of hybrid multi-source system. The gain values of both inner and outer loop controllers are tuned simultaneously by the hybrid PSO-GSA algorithm. The design problem is conceptualized as constrained optimization problem of minimizing the steady state error index IAE as shown below,

$$\min(\mathrm{J}) = \int_0^t \{|\mathrm{ACE_i}|\}dt = \int_0^t \left\{|\Delta f_i| + \left|\Delta P_{\mathrm{tie},i-j}\right|\right\}dt \tag{43}$$

Subjected to:

$$K_{pj}^{\min} \le K_{pj} \le K_{pj}^{\max}$$
$$K_{ij}^{\min} \le K_{ij} \le K_{ij}^{\max}$$
$$K_{dj}^{\min} \le K_{dj} \le K_{dj}^{\max}$$

where j is the area number varying from 1, 2, 3 . . . n with $j \neq i$. $K_{pj}^{\min}$, $K_{pj}^{\max}$, $K_{ij}^{\min}$, $K_{ij}^{\max}$, $K_{dj}^{\min}$ and $K_{dj}^{\max}$ are the minimum and maximum bounds of controller gain parameters. The minimum and maximum bounds for gains of controller are chosen by several trial run as -100 and 10, respectively.

IV. PARTICLE SWARM OPTIMIZATION-GRAVITATIONAL SEARCH ALGORITHM (PSO-GSA)

PSO-GSA is a co-evolutionary heterogeneous hybrid optimization method used to obtain the global optimal solution. PSO algorithm is used to optimize the gravitational constant of GSA and thus improving the search ability of the algorithm. The hybrid approach integrates the exploration characteristics of PSO with the exploitation behavior of GSA algorithm to obtain the global optimum. In this paper, the hybrid method was used to tune the gain values of the controller for ALFC application to minimize the frequency error of the interconnected HPS. The proposed algorithm is detailed as follows [39], [43]:

Step-1: The inputs of gains of controller are initialized randomly. These gain parameters are called as agents and its random position is represented as

$$X_i = (xi^1, \ldots x_i{}^d, \ldots x_i{}^n)$$

for $i = 1, 2 \ldots N$. Where, $x_i{}^d$ is the position of i^{th} agent in d dimension, n is the search space dimension of the problem.

Step-2: Compute the fitness function to be minimized using (43) for all agents.

Step-3: The masses of the agents are initialized randomly and the forces acting between the agent i and j is calculated as

$$F_{ij}^d(s) = G(t)\frac{M_i(t) \cdot M_j(t)}{R_{ij}(t) + \in}(x_j{}^d(t) - x_i{}^d(t)) \tag{44}$$

where, $M_j(t)$ is the active gravitational mass related to agent j, $M_i(t)$ is the passive gravitational mass related to agent i, $G(t)$ is the gravitational constant at time t, $\in$ is the small constant, x_i and x_j are the i^{th} and j^{th} positions of agent. $R_{ij}(t)$ is the euclidean distance between two agents i and j given by

$$R_{ij}(t) = \left\| X_i(t), X_j(t) \right\|_2 \tag{45}$$

The gravitational constant $G(t)$ is defined as

$$G(t) = G_o \times e^{\left(-\alpha \times \frac{\text{iter}}{\max(\text{iter})}\right)} \tag{46}$$

where G_o is the initial value and α is the descending coefficient. The total forces that acting on agent is

$$F_i^d(t) = \sum_{j=1, j\neq i}^{n} \text{rand}_j F^d{}_{ij}(t) \tag{47}$$

where rand_j is the random number belongs to [0,1]. The acceleration of i^{th} agent is given by,

$$a_i^d(t) = \frac{F_i{}^d(t)}{M_{ii}(t)} \tag{48}$$

where $M_{ii}(t)$ is the inertia mass of i^{th} agent.

Step-4: The gravitational parameters such as gravitational constant $G(t)$ and acceleration of i^{th} agent $a_{\text{i}}{}^{\text{d}}(t)$ are optimized by the PSO algorithm and the steps for PSO algorithm are described in Step 5.

Step-5: The shortest form of PSO algorithm is portrayed for better understanding of the hybrid algorithm. The position and velocity of all controlling parameters of PSO algorithm are initialized randomly. Here, every parameter is viewed as particle and the position vector at k^{th} iteration as

$$y_i{}^k = (y_{i1}^k, \ldots y_{i2}^k, \ldots y_{in}^k)$$

(a) The velocity vector at k^{th} iteration is defined as

$$v_i{}^k = (v_{i1}^k, \ldots v_{i2}^k, \ldots v_{in}^k)$$

(b) The best solution obtained at k^{th} iteration is defined as $P_{k\text{best}}$

(c) Evaluate the objective function of the particles

$$\min(g(k)) \tag{49}$$

where $g(k)$ is the gravitational constant function defined in (46) and controlled by (47).

(d) Now, the personal best $P_{k\text{best}}$ of every particle is compared with its current fitness value and update the $P_{k\text{best}}$ coordinates. Similarly, the current fitness value is compared with $g_{k\text{best}}$ and also update the $g_{k\text{best}}$ coordinates.

(e) The obtained $g_{k\text{best}}$ is the optimal value of acceleration, a_d^i. Now, this value is used for updating the velocity vector of GSA algorithm.

Step-6: In this step, the obtained acceleration constant from PSO algorithm has been used to update the velocity and position of an agent using the following equations,

$$V_k^{i+1} = wV_i{}^i + c_1{}' \times \text{rand} \times a_d^i + c_2{}' \times \text{rand} \times \left(g_{\text{best}} - x_k^i\right) \tag{50}$$

$$x_k^{i+1} = x_k^i + V_k^{i+1} \tag{51}$$

Step-7: When the change in fitness value is reaching the tolerance limit of $\tau = 0.0001$, obtain the optimised gain values of the controller. Else repeat the step from 2 to 7 until the terminating condition is reached.

Thus, the object with heavier mass gives the best solution and the one with lighter mass results in the worst solution. Hence, the position of the object gives the solution and every particle possesses mass, velocity and acceleration. The parameters initialized for the proposed method are: maximum iteration = 100, population size = 10, inertia weight $w = [0, 1]$, $c_1' = 0.5$, $c_2' = 1.5$, gravitational constant $G_{\text{o}} = 1$, $\alpha = 2$, rand is the random number belongs to [0,1], lower bound = −100 and upper bound = 10. The detailed procedure for tuning the gains of controller is also represented in Figure 3. The tuned values of controller gain parameters obtained by the proposed PSO-GSA technique is given in Table 1.

V. RESULTS AND DISCUSSION

This section describes the dynamic response of multi-area HPS for I, PI, PID, IPD, and cascade PI-PD controllers. The efficiency of various controllers was studied for different combination of generating sources and load disturbance by optimizing the gain values of controller using hybrid PSO-GSA based optimization method. In this approach, the IAE criterion was used to optimize the gains of the controller for various cases of the system model and the results are discussed in the forthcoming sections.

Case 1: In this case, it is assumed that the thermal generating source is operating in both the areas of the system. A step load increase of 0.01 p.u. and 0.0125 p.u. of plant capacity were considered in area 1 (A1) and area 2 (A2), respectively. The power system frequency and tie-line power fluctuations recorded for I, PI, PID, IPD, and cascade PI-PD controllers are shown in Figure 4. These deviations were controlled by tuning the gain values of controller and the system response was adjusted in accordance with the error IAE as it becomes infinitesimal value. From the results, the oscillations were quickly damped out by the cascade PI-PD controller compared to those of the other classical

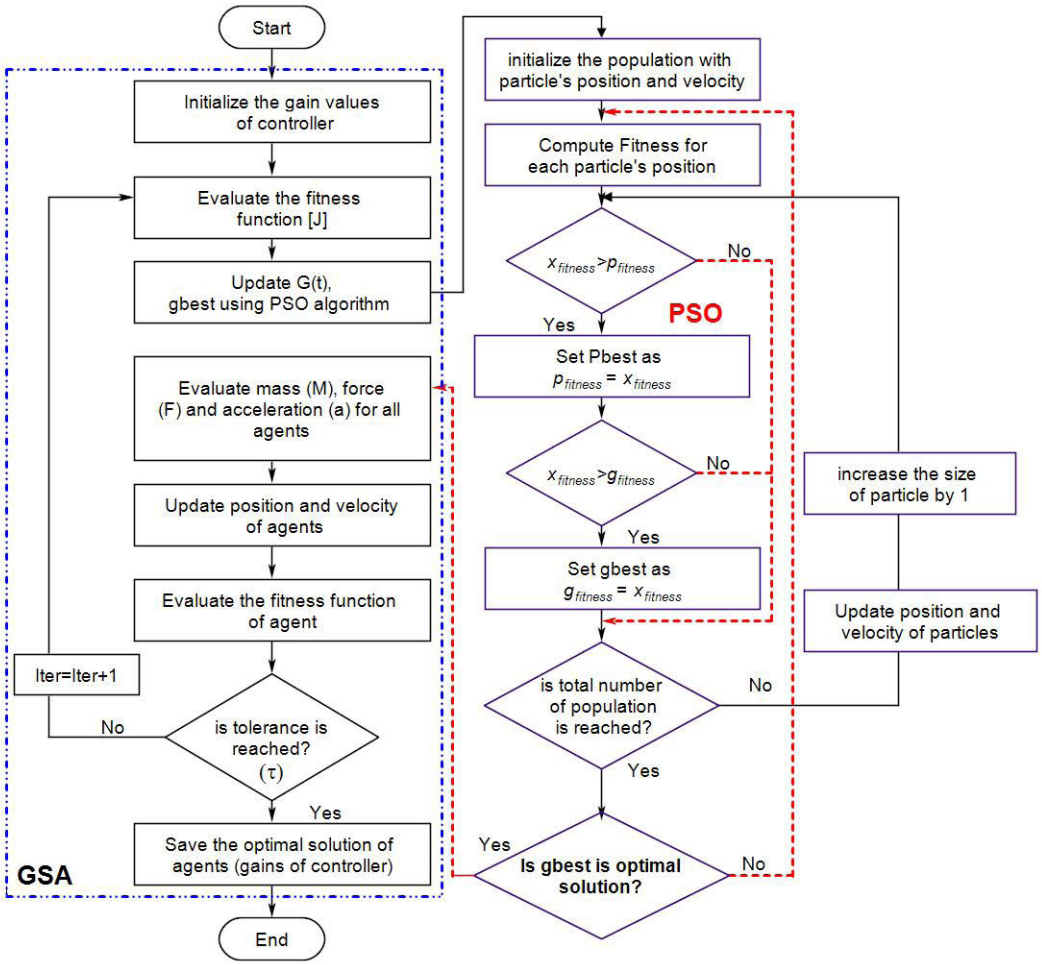

FIGURE 3. PSO-GSA method of optimizing controller parameters.

controllers. This is because, the inner loop of the cascade control scheme responded very fast to the change in the load demand. The results indicate that the single loop controllers have a phase-lag in responding to the system disturbances compared to the cascade control system.

Case 2: In this case, the two-area system consists of thermal, hydro, and gas power generation sources and the increase in the load demand was considered as in Case 1. The increase in power generation was considered by the addition of hydro and gas power generation into the system. Thus, the power generation is expressed as:

$$P_s = P_{\text{Thermal}} + P_{\text{Hydro}} + P_{\text{Gas}} \tag{52}$$

The generation was adjusted automatically to change the load demand. The dynamic frequency and tie-line power response of two-area multisource system during the load change is presented in Figure 5. The result shows that the dynamics in frequency with increased load in Case 2 were reduced more than those of in Case 1. From the results, the oscillations in frequency deviation and tie-line power fluctuation were damped out rapidly for the proposed cascade PI-PD controller compared to those of the other classical controllers. Furthermore, the efficiency of the controller was studied for random change in load demand as portrayed in Figure 6. Figure 7 shows that the cascade PI-PD controller outperformed than other classical controllers by settling rapidly to steady state with minimum overshoots/undershoots in the dynamic response of frequency and tie-line power variation for random change in load. The gain values obtained under this case by PSO-GSA method of tuning for various controllers are presented in Table 1.

Case 3: In this case, the two-area HPS model comprises of conventional reheat thermal power system interconnected with RE sources such as wind, DEG, AE, FC, and BESS. Initially, a SLP similar to Case 1 was considered with wind power generation of 0.1 p.u. The frequency and tie-line power deviation for load change are presented in Figure 8. From the figure, the fluctuations in the dynamic responses were slightly reduced and the frequency reached the steady state compared to those of in Case 1. In addition, to study the efficiency of controller, random variation in load demand and wind power generation were considered and depicted as

TABLE 1. Controller gains for various cases.

Type of Controller	Gains	Case 1	Case 2	Case 3	Case 4	
		A1=A2	A1=A2	A1=A2	A1	A2
I	K_i	-0.4053	-4.9449	-0.1942	-0.5099	-0.8
PI	K_p	-0.0257	-0.05275	-0.0363	-0.03732	-0.0262
	K_i	-0.3071	-6.236	-0.1492	-1	-6.258
PID	Kp	-4.69	-2.9418	-4.2765	-1.6433	-4.0843
	K_i	-3.0271	-10	-2.8447	-10	-6.4789
	K_d	-1.9355	-1.2209	-2.3836	-1.0386	-1.1288
IPD	K_i	-2.5019	-3.2	-2.0349	-3	-2.986
	K_p	1.1484	-3	3	2.7786	-2.6228
	K_d	1.5364	-0.0376	2.9186	0.9096	-0.5552
PI-PD	K_p	0.115	-3.9975	-24.882	2.9935	-3
	K_i	-2.486	-15	-65	3	-2.9998
	K_{p1}	2.71	5	-10	0.4678	3
	K_d	2.3283	3.4306	-10	-3	-0.5199

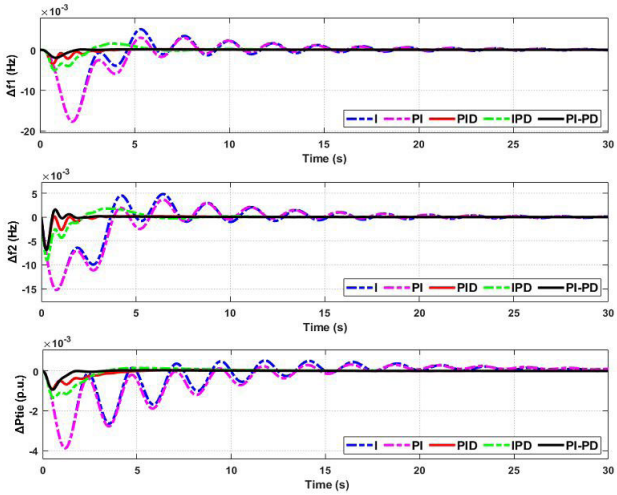

FIGURE 4. Dynamic response of two-area thermal power system.

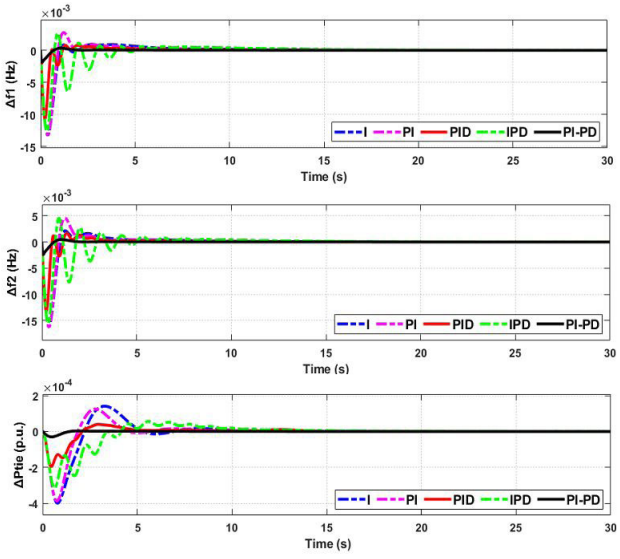

FIGURE 5. Dynamic response of two-area multi-source power system.

in Figures 6 and 9, respectively. The frequency and tie-line power responses for these random changes are portrayed in Figures 11 and 12. The results show that the proposed cascade PI-PD controller responded abruptly for sudden increase/decrease in load or wind power generation compared to other classical controllers. The tie-line power also varied largely for the change in load demand of the system and maintained the steady state for the change in wind power generation. Thus, the change in wind power generation was balanced by the energy storage and diesel power generation of interconnected HPS. To test the robustness of the controller for HPS, the effect of change in load demand and wind power generation were considered simultaneously as given in Figure 10. The frequency and tie-line variations during these simultaneous changes in load and wind power generation are illustrated in Figure 13. The results indicate that the cascade control outperformed than other classical controllers with minimum overshoot/undershoot for uncertain disturbances. The lack of oscillations during power

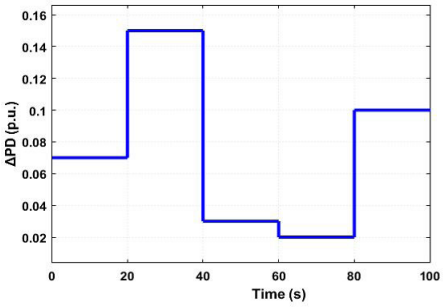

FIGURE 6. Random Load Change.

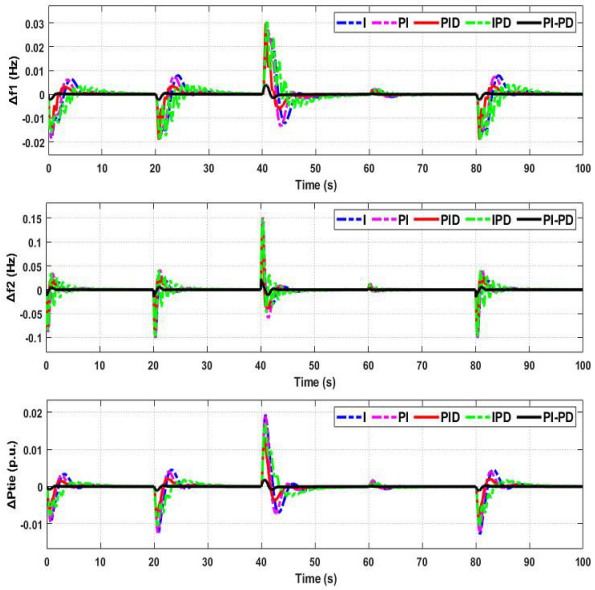

FIGURE 7. Dynamic response of two-area multi-source system for random load change.

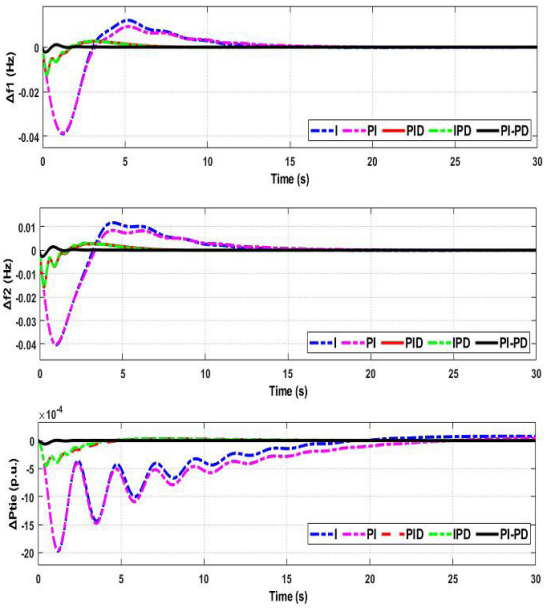

FIGURE 8. Dynamic response of two-area HPS.

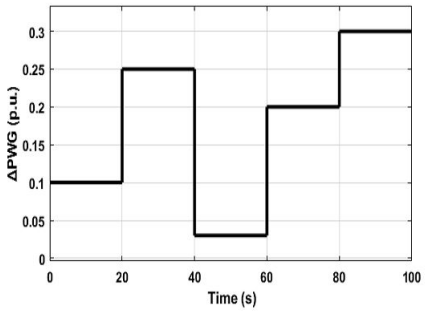

FIGURE 9. Random Load change in wind power generation.

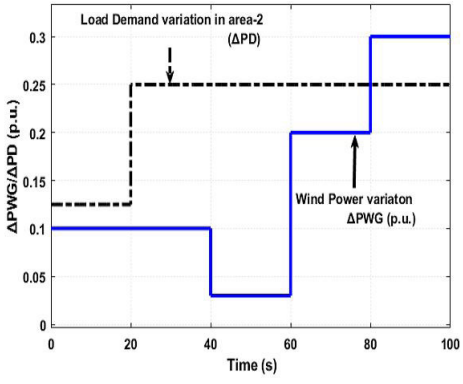

FIGURE 10. Random Change in wind power generation and load demand.

generations indicating the balance condition of the system and the total power generation of interconnected HPS is expressed as follows:

$$P_s = P_{\text{Thermal}} + P_{\text{Wind}} + P_{\text{DEG}} - P_{\text{AE}} + P_{\text{FC}} \pm P_{\text{BESS}} \tag{53}$$

Case 4: In this case, the two unequal areas with area 1 comprises of reheat thermal, hydro, and gas power generations and area 2 consists of reheat thermal and RE sources such as wind, DEG, AE, FC, and BESS were considered. Similar to Case 1, the increase in the load demand of 0.01 p.u. and 0.0125 p.u. pertaining to area 1 and area 2, respectively, were considered. The total power generation of interconnected HPS is as follows:

$$P_s = P_{\text{Thermal}} + P_{\text{Hydro}} + P_{\text{Gas}} + P_{\text{Wind}} + P_{\text{DEG}} - P_{\text{AE}} + P_{\text{FC}} \pm P_{\text{BESS}} \tag{54}$$

The result proves that the system has excessive generation to meet the increasing load demand and the frequency overshoot/oscillations were damped out by the properly tuned controller. The tuned gain values of controllers using PSO-GSA method are given in Table 1. The dynamic response of unequal two-area system for step change in load demand is given in Figure 14. It is seen that the system

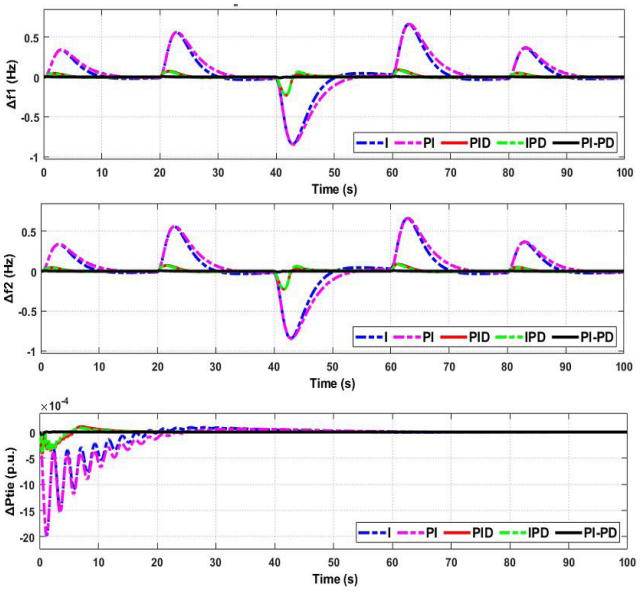

FIGURE 11. Dynamic response of two-area HPS for random change in wind power generation.

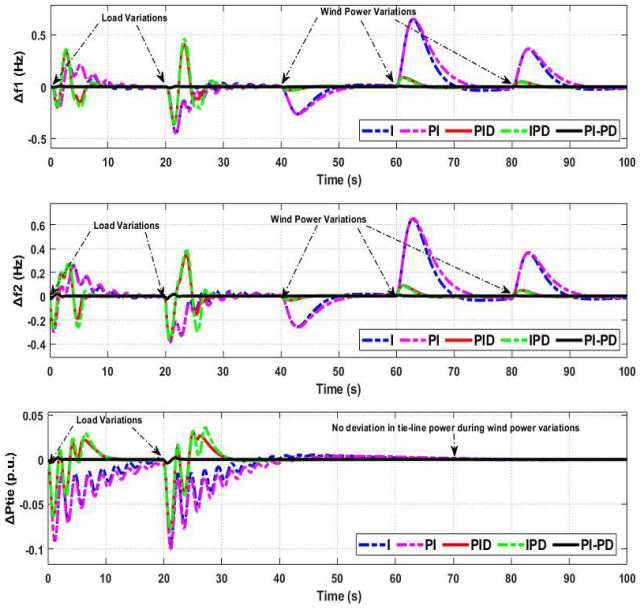

FIGURE 13. Dynamic response of HPS for random change in wind power generation and load demand.

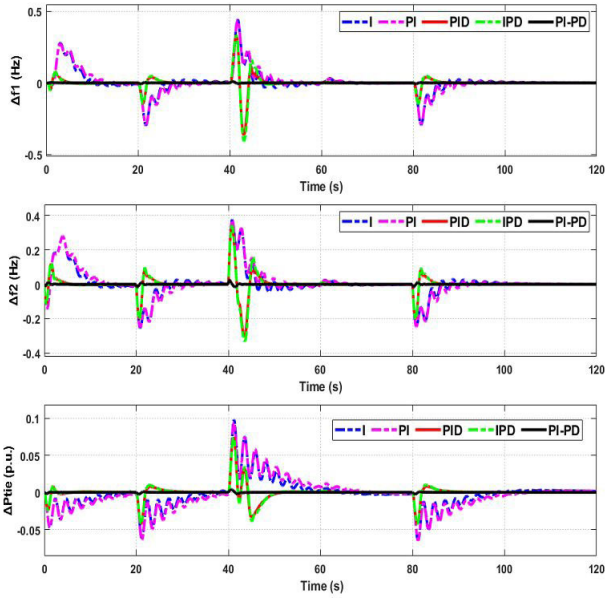

FIGURE 12. Dynamic response of two-area HPS for random change in load.

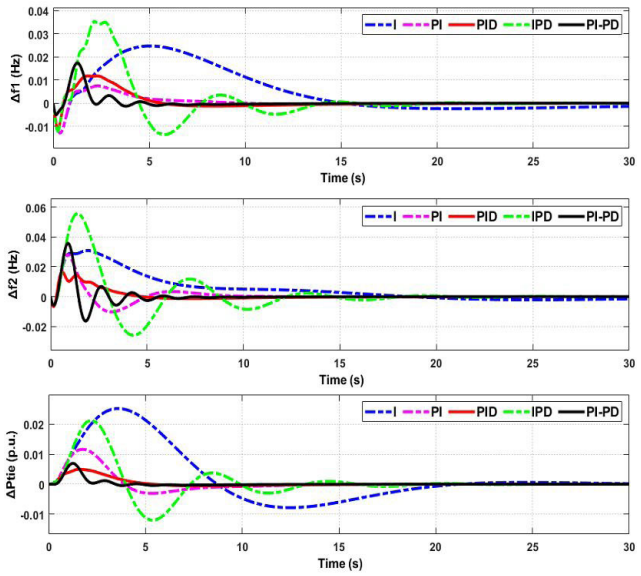

FIGURE 14. Dynamic response of two unequal area HPS.

drives back to steady state from its transient state quickly by the cascade controller compared to the other classical controllers. Moreover, the robustness of the controller was validated for uncertain change in the load demand and wind power variations as portrayed in Figure 10. The dynamic response of system frequency and tie-line power variation for these changes are illustrated in Figure 15. The results show that the cascade PI-PD controller eradicated the fluctuations and drove the system back to steady state quickly for these uncertain changes. The tie-line power also fluctuated for the perturbation in wind power unlike in Case 3. Thus, the existence of oscillation is because of the two unequal areas of HPS and the excess power generated by wind plant is stored by the storage devices in area 2. On the other hand, the excessive power generation by conventional generators (thermal, hydro, and gas) in area 1 is supplied to area 2 through the tie-line that leads to the oscillation in the tie-line, and this is minimized by the designed robust cascade controller.

A. PERFORMANCE ANALYSIS OF CONTROLLER

This section describes the performance analysis of various classical controllers for disparate combination of

TABLE 2. Settling and Rise time of frequency deviation in area 1.

Cases	△f1									
	Settling Time (s)					Rise Time (s)				
	I	PI	PID	IPD	PI-PD	I	PI	PID	IPD	PI-PD
1	15.1954	17.267	12.0706	10.8677	6.8916	0.0005	0.0073	0.0099	0.0002	0.00008
2	6.8877	5.6694	5.0821	10.8774	1.8691	0.0003	0.0001	0.0001	0.0001	0.00001
3	21.7183	13.6446	17.9422	17.2287	9.8115	0.0182	0.0229	0.0005	0.0004	0.00001
4	26.4666	21.4132	17.2673	18.6184	12.0925	0.0297	0.00003	0.0003	0.0012	0.00006

TABLE 3. Settling and Rise time of frequency deviation in area 2.

Cases	△f2									
	Settling Time (s)					Rise Time (s)				
	I	PI	PID	IPD	PI-PD	I	PI	PID	IPD	PI-PD
1	16.0886	16.4488	10.7074	10.637	5.7285	0.0051	0.0202	0.0018	3.42×10^{-4}	2.98×10^{-4}
2	7.0963	5.8163	3.509	10.8774	1.8691	0.0001	0.00009	4.69×10^{-5}	1.11×10^{-4}	1.36×10^{-4}
3	22.0062	13.8043	17.7898	17.0713	9.0265	0.0141	0.0177	4.39×10^{-4}	3.59×10^{-4}	1.49×10^{-5}
4	19.7199	8.7227	14.8234	17.3455	7.4488	0.0316	1.93×10^{-5}	2.00×10^{-4}	8.37×10^{-5}	1.83×10^{-5}

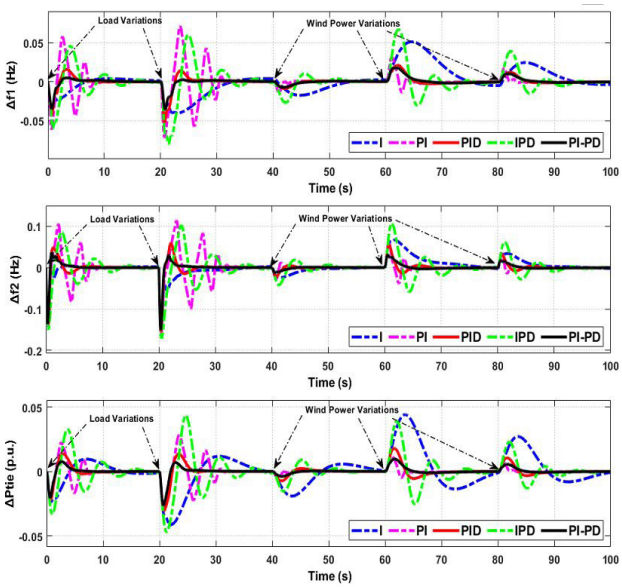

FIGURE 15. Dynamic response of two unequal area HPS for random change in wind power generation and load demand.

generating sources (Cases 1 to 4) considered to study the efficiency of multi-loop control scheme over single-loop feedback control for ALFC applications of HPS. Tables 2 to 12 depict the transient performance indices of settling time, rise time, peak magnitude, peak-overshoot, peak-undershoot and control effort, and steady state performance indices of IAE, ITAE, ISE, and ITSE for various cases of operation in multi-area HPS. The results indicate that the settling time was reduced almost half of its value for the proposed CCs and the amount of reduction varied from 20% to 60% for various cases of HPS operation than those of the I, PI, PID, and IPD controllers. Similarly, the rise and peak time were significantly declined by 5% to 20% and 30% to 70%, respectively, for the cascade PI-PD controller than those of the other controllers for all the cases. The peak magnitude and control effort were also decreased by 10% to 90% for the CCs than those of the single loop controllers under various disparate cases of the system. Comparably, the peak-undershoot and overshoots are also reduced by a proportion of 21% to 92% and 2% to 90%, respectively. In addition, the proposed CCs also shows significant improvement in the steady state performance indices with 30% to 95% reduction of ISE and IAE, respectively, and 10% to 90% reduction of ITSE and ITAE indices than those of the I, PI, PID, and IPD controllers for different cases of HPS operation.

B. SENSITIVITY ANALYSIS OF PI-PD CONTROLLER

The sensitivity analysis of the controller was carried out to test the robustness of optimum gains of PI-PD controller

TABLE 4. Peak time and magnitude of frequency deviation in area 1.

Cases	Δf1									
	Peak Time (s)					|Peak Magnitude|				
	I	PI	PID	IPD	PI-PD	I	PI	PID	IPD	PI-PD
1	1.5289	1.5289	0.294	0.4192	0.2794	0.0594	0.0599	0.0144	0.0358	0.0142
2	0.3935	0.3935	0.2234	0.3113	0.0738	0.0132	0.0132	0.0108	0.0157	0.0024
3	3.1802	3.2	1.8402	1.7794	0.73	0.1512	0.1509	0.0198	0.0189	0.0026
4	4.9089	2.3387	2.2663	2.1615	1.3613	0.0392	0.0136	0.0179	0.0548	0.0128

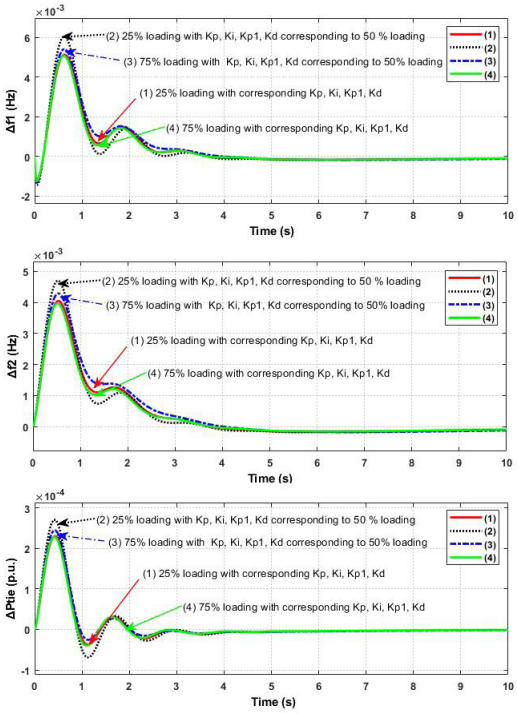

FIGURE 16. Comparison of dynamic response of system for change in system loading (25% and 75% with corresponding K_p, K_i, K_{p1}, K_d and, 25 and 75% loading with K_p, K_i, K_{p1}, K_d corresponding to nominal 50% loading).

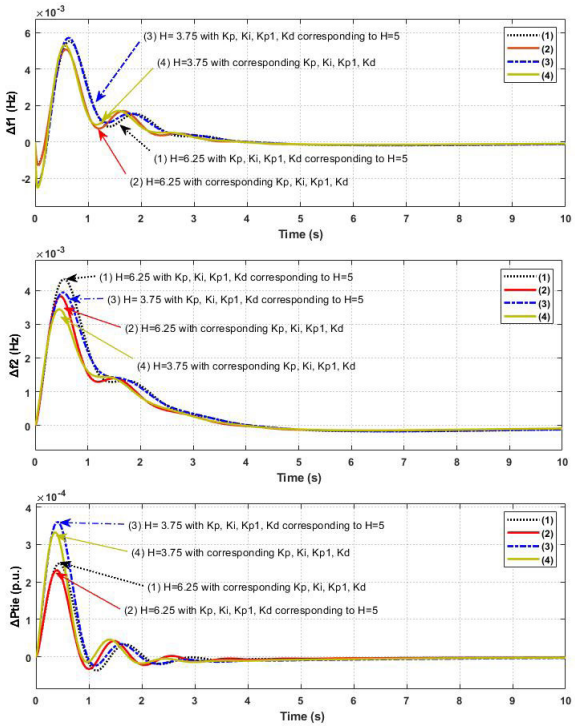

FIGURE 17. Comparison of dynamic response of system for change inertia of system (±25% of H (=5) with corresponding K_p, K_i, K_{p1}, K_d and, ±25% of H with K_p, K_i, K_{p1}, K_d corresponding to nominal $H = 5$).

obtained under nominal loading of system (50% loading), nominal SLP for wide variation in system loading, and nominal inertia constant ($H = 5$) of the system.

In this analysis, the system parameters such as loading, SLP and nominal inertia constant of the system were perturbed, and the corresponding gain values of the controller were obtained using the PSO-GSA method. The change in the loading conditions affects the time constant, T_{ps} and gain constant, K_{ps} of power system block, which in turn has impact on frequency and tie-line power response. Similarly, the change in inertia of the system H has adverse impact on time constant T_{ps} of the system. Thus, the newly tuned values of the controller obtained under these changes are portrayed in Table 13. Figures 16 to 18 represent the dynamic response of system with the optimum gain values obtained at the aforementioned conditions, compared to the response of gain values K_p, K_i, K_{p1} and K_d obtained at nominal conditions. From the results, the response obtained were similar to the gain values obtained under nominal conditions and change in system parameter conditions. Thus, the result shows a good tolerance for wide change in system parameters for the gain values obtained at nominal conditions. Hence, it can be concluded that the parameters are not needed to be re-tuned for wide variations in system parameters and conditions.

TABLE 5. Peak time and magnitude of frequency deviation in area 2.

Cases	Δf2									
	Peak Time (s)					|Peak Magnitude|				
	I	PI	PID	IPD	PI-PD	I	PI	PID	IPD	PI-PD
1	1.2786	1.3157	0.2857	0.4425	0.2774	0.0564	0.0566	0.0176	0.0429	0.0175
2	0.3492	0.3492	0.2234	0.3113	0.0738	0.0162	0.0162	0.0134	0.0157	0.0024
3	3.3	3.443	1.9783	1.9392	0.73	0.1486	0.1492	0.0206	0.0197	0.003
4	1.8734	0.8629	0.5785	1.3332	0.5702	0.0501	0.0438	0.0256	0.0863	0.0255

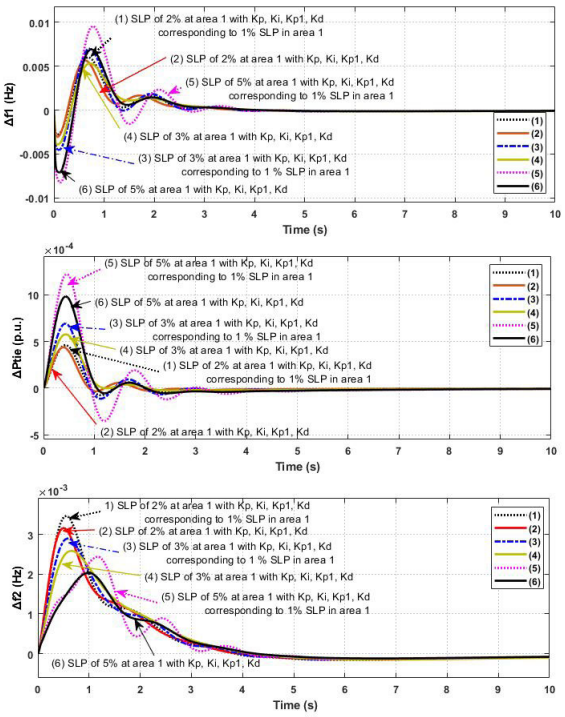

FIGURE 18. Comparison of dynamic response of system for change SLP of system (2%, 3%, 5% of SLP in area 1 with corresponding K_p, K_i, K_{p1}, K_d and, 2%, 3%, 5% of SLP in area 1 with K_p, K_i, K_{p1}, K_d corresponding to nominal 1% of SLP in area 1).

VI. STABILITY ANALYSIS

To analyze the stability of multi-area HPS with proposed cascade controller, a generalized i^{th} pool of interconnected power system was considered. The inner PD controller responds to frequency deviation due to the sudden change in load demand and the outer PI controller acts for any change in frequency and tie-line power of the system. The generalized control block diagram representing Figure 1 is depicted in Figure 19. The plant transfer function, $G_1(s)$ and $G_2(s)$ were taken as the power system and governor-turbine nonlinear model integrated with RE sources and energy storage system.

The CLTF of the system for the proposed controller pertaining to change in load demand (ΔP_D) is expressed as:

$$\Delta f = \frac{-G_1}{1 + G_1 G_2 \left[C_2 + \frac{1}{R_i} - B_i C_1 C_2\right]} \Delta P_D \tag{55}$$

The CLTF applicable to change in tie-line power variation is defined as:

$$\Delta f = \frac{G_1 G_2 C_1 C_2}{1 + G_1 G_2 \left[C_2 + \frac{1}{R_i} - B_i C_1 C_2\right]} \Delta P_{\text{tie}} \tag{56}$$

In general, the CLTF for change in both load demand and tie-line power variation are obtained by superposition principle and can be defined as,

$$\Delta f = \frac{-\left[(G_1)\,\Delta P_D + (G_1 G_2 C_1 C_2)\,\Delta P_{\text{tie}}\right]}{1 + G_1 G_2 \left[C_2 + \frac{1}{R_i} - B_i C_1 C_2\right]} \tag{57}$$

In lineralizing the system model and simplifying the analysis for Case 1 of thermal system generation, the CLTF pertaining to the load demand in area 1 can be expressed using the state space analysis presented in Section 2 as,

$$\text{CLTF}_{(\text{case}-1)} = \frac{\text{num}}{\text{den}} \tag{58}$$

where num and den are defined in Appendix.

The state space matrix of the above CLTF in (58) for obtaining the reduced order model of the system are given in Appendix. To study the stability of proposed work, the higher order plant transfer function was reduced to second-order transfer function by retaining the dominant poles of the system using Hankel matrix method [48], [49]. The Hankel matrix can be obtained from the state space matrix given in Appendix. The Hankel matrix in general form can be expressed as:

$$H_{nn}^{(0)} = \begin{bmatrix} CB & CA^{-1}B & \dots & \dots & CA^{-n+1}B \\ CA^{-1}B & CA^{-2}B & \dots & \dots & CA^{-n}B \\ \dots & \dots & \dots & \dots & \dots \\ CA^{-n+2}B & CA^{-n+1}B & \dots & \dots & CA^{-2n+3}B \\ CA^{-n+1}B & CA^{-n}B & \dots & \dots & CA^{-2n+2}B \end{bmatrix} \tag{59}$$

TABLE 6. Peak-Undershoots and Overshoots of frequency deviation in area 1.

Cases	Δf1									
	Peak-Undershoots					Peak-Overshoots				
	I	PI	PID	IPD	PI-PD	I	PI	PID	IPD	PI-PD
I	0.0594	0.0599	0.0144	0.0189	0.0113	0.0111	0.0058	0.0007	0.0073	0.0005
II	0.0132	0.0132	0.0108	0.0127	0.0019	0.0008	0.0028	0.0007	0.0029	0.0003
III	0.0187	0.0088	0.0056	0.0057	0.0014	0.3387	0.3397	0.0447	0.0425	0.0048
IV	0.0126	0.0126	0.0108	0.0211	0.005	0.0392	0.0125	0.0179	0.055	0.0128

TABLE 7. Peak-Undershoots and Overshoots of frequency deviation in area 2.

Cases	Δf2									
	Peak-Undershoots					Peak-Overshoots				
	I	PI	PID	IPD	PI-PD	I	PI	PID	IPD	PI-PD
I	0.0564	0.0566	0.0176	0.0226	0.0174	0.0101	0.0057	0.0008	0.0074	0.0006
II	0.0162	0.0162	0.0134	0.0157	0.0024	0.0021	0.0045	0.0018	0.0049	0.0004
III	0.0191	0.0089	0.0084	0.0085	0.0018	0.3351	0.3365	0.044	0.0414	0.0051
IV	0.0044	0.0141	0.0049	0.0401	0.0135	0.0501	0.0438	0.0255	0.0864	0.0225

TABLE 8. ISE and ITSE of frequency deviation in area 1.

Cases	Δf1									
	ISE					ITSE				
	I	PI	PID	IPD	PI-PD	I	PI	PID	IPD	PI-PD
1	0.0061	0.0066	0.0001	0.0005	6.73×10^{-5}	0.1829	0.1983	0.0041	0.0164	0.002
2	8.10×10^{-5}	7.945×10^{-5}	3.02×10^{-5}	7.77×10^{-5}	8.98×10^{-7}	0.0024	0.0024	0.0009	0.0023	2.69×10^{-5}
3	0.0736	0.0842	0.0009	0.0007	4.18×10^{-6}	2.21	2.529	0.0271	0.0232	0.0001
4	0.0089	0.0004	0.0007	0.0063	0.0003	0.2683	0.012	0.0215	1.883	0.0206

Here, the order of the transfer function is 13, therefore n = 13. The above matrix (59) can be expressed in Hankel form as below:

$$H_{1313}^{(0)} = \begin{bmatrix} e_{11} & e_{12} & e_{13} & \dots & e_{1n} \\ e_{21} & e_{22} & e_{23} & \dots & e_{2n} \\ e_{31} & e_{32} & e_{34} & \dots & e_{3n} \\ \dots & \dots & \dots & \dots & \dots \\ e_{n1} & e_{n2} & e_{n3} & \dots & e_{nn} \end{bmatrix} \tag{60}$$

The simplified form of (60) is represented as:

$$H_{1313}^{(0)} = \begin{bmatrix} H_1^{(0)} & H_2^{(0)} \end{bmatrix} \tag{61}$$

where $H_1^{(0)}$ and $H_2^{(0)}$ are given in Appendix. The Hankel matrices in Hermite normal form can be represented as:

$$H_{1313}^{(1)} = H_{1313}^{(0)} - \frac{1}{e_{11}} \begin{bmatrix} z \\ e_{21} \\ e_{31} \\ \dots \\ e_{n1} \end{bmatrix} \begin{bmatrix} e_{11} & e_{12} & e_{13} & \dots & e_{1n} \end{bmatrix} \tag{62}$$

$$H_{1313}^{(1)} = \begin{bmatrix} 1 & e_{12}' & e_{13}' & \dots & e_{1n}' \\ 0 & e_{22}' & e_{23}' & \dots & e_{2n}' \\ 0 & e_{32}' & e_{33}' & \dots & e_{3n}' \\ \dots & \dots & \dots & \dots & \dots \\ 0 & e_{n2}' & e_{n3}' & \dots & e_{nn}' \end{bmatrix} \tag{63}$$

TABLE 9. ISE and ITSE of frequency deviation in area 2.

Cases	Δf2									
	ISE					ITSE				
	I	PI	PID	IPD	PI-PD	I	PI	PID	IPD	PI-PD
1	0.0061	0.0066	0.0001	0.0006	9.11×10^{-5}	0.1828	0.1984	0.0046	0.0174	0.0027
2	0.0001	0.0001	4.56×10^{-5}	0.0001	1.31×10^{-6}	0.0035	0.0035	0.0014	0.0035	3.94×10^{-5}
3	0.0741	0.0847	0.0009	0.0008	5.29×10^{-6}	2.223	2.542	0.0282	0.0244	0.0001
4	0.0085	0.0017	0.0007	0.0124	2.10×10^{-4}	0.2569	0.0504	0.0234	0.3743	0.0063

TABLE 10. IAE and ITAE of frequency deviation in area 1.

Cases	Δf1									
	IAE					ITAE				
	I	PI	PID	IPD	PI-PD	I	PI	PID	IPD	PI-PD
1	0.082	0.1084	0.0109	0.0133	0.0049	2.46	3.253	0.329	0.3978	0.1478
2	0.0033	0.0025	0.0016	0.005	0.0002	0.0981	0.0777	0.0484	0.1517	0.0064
3	0.5891	0.7688	0.0398	0.0345	0.0015	17.67	23.06	1.196	1.035	0.0456
4	0.2474	0.0247	0.0303	0.0647	0.0208	7.422	0.7418	0.9087	1.943	0.6257

TABLE 11. IAE and ITAE of frequency deviation in area 2.

Cases	Δf2									
	IAE					ITAE				
	I	PI	PID	IPD	PI-PD	I	PI	PID	IPD	PI-PD
1	0.082	0.1083	0.0109	0.0132	0.0049	2.459	3.249	0.329	0.3978	0.1478
2	0.0033	0.0025	0.0016	0.0051	0.0002	0.098	0.0777	0.0484	0.1516	0.0064
3	0.5893	0.7689	0.0398	0.0345	0.0012	17.68	23.07	1.196	1.035	0.0456
4	0.2478	0.0246	0.0303	0.0646	0.0208	7.435	0.7407	0.908	1.939	0.6252

On solving $H^{(1)}_{1313}$ using the elements of matrix $H^{(0)}_{1313}$ is expressed as:

$$H^{(1)}_{1313} = \begin{bmatrix} H^{(1)}_3 & H^{(1)}_4 \end{bmatrix} \tag{64}$$

where $H^{(0)}_3$ and $H^{(0)}_4$ are given in Appendix. As similar to $H^{(1)}_{1313}, H^{(2)}_{1313}$ in hermite normal form is,

$$H^{(1)}_{1313} = H^{(0)}_{1313} - \frac{1}{e_{11}} \begin{bmatrix} z \\ e_{21} \\ e_{31} \\ \dots \\ e_{n1} \end{bmatrix} \begin{bmatrix} e_{11} & e_{12} & e_{13} & \dots & e_{1n} \end{bmatrix} \tag{65}$$

On solving $H^{(2)}_{1313}$ using the elements of matrix $H^{(1)}_{1313}$ is expressed as:

$$H^{(2)}_{1313} = \begin{bmatrix} H^{(2)}_5 & H^{(2)}_6 \end{bmatrix} \tag{66}$$

where $H^{(0)}_5$ and $H^{(0)}_6$ are given in Appendix.

Thus, the reduced order function obtained by solving the state space parameter using the elements (state matrix form) of Hermite form $H^{(2)}_{1313}$ is as follows,

$$A_2 = \begin{bmatrix} -8.885 & -35.49 \\ 1 & 0 \end{bmatrix}$$

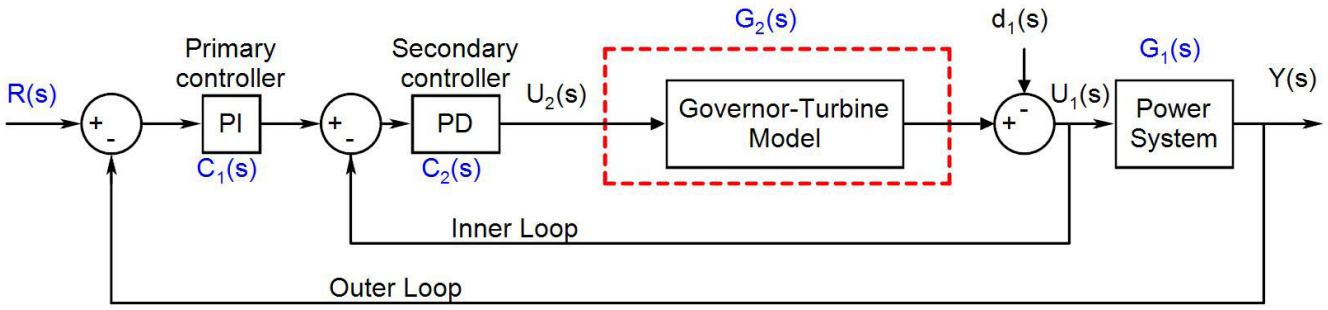

FIGURE 19. Closed loop analysis of simple power system model.

TABLE 12. Control Effort.

Cases	Control Effort (Joules)									
	Δf1					Δf2				
	I	PI	PID	IPD	PI-PD	I	PI	PID	IPD	PI-PD
1	3.752	4.5055	1.6373	1.9915	1.4664	4.0857	4.837	1.9473	2.3481	1.7775
2	0.0819	0.0663	0.0762	0.1355	0.0061	0.0819	0.0177	0.0728	0.0783	0.005
3	17.8221	23.3944	1.3474	1.1852	0.0765	17.7467	23.3176	1.3428	1.1811	0.078
4	6.9238	2.4881	1.2177	3.1025	0.1588	12.8955	5.2571	3.9611	9.9494	0.8271

TABLE 13. Gain values of the controller obtained for sensitive analysis.

Controller	Gains	25% Loading	75% Loading	H=6.25	H=3.75	2% SLP in Area 1	3% SLP in Area 1	5% SLP in Area 1
PI-PD	K_p	-5	4.9574	-5	5	-5	4.8313	4.1731
	K_i	-4.9849	5	-2.4973	4.8532	-1.2016	-2.4893	2.347
	K_{p1}	-0.2032	-0.2424	4.005	4.1734	-5	-4.5348	3.6781
	K_d	-5	-4.193	-4.0645	2.3447	-3.3969	1.7284	-5

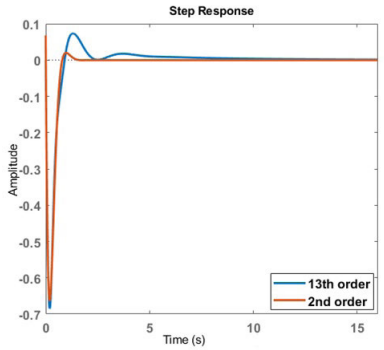

FIGURE 20. Step response of original and reduced order model.

$$B_2 = \begin{bmatrix} 1 \\ 0 \end{bmatrix}$$

$$C_2 A_2^{-1} = \begin{bmatrix} 0.0677 & -8.918 \end{bmatrix}$$

Hence, the reduced order transfer function obtained for Case 1 using state space matrix and is defined as,

$$\text{CLTF}_{(\text{case}-1)} = \frac{0.06768s^2 - 8.918s + 2.535 \times 10^{-13}}{s^2 + 8.885s + 35.49} \tag{67}$$

The step-response obtained for the original 13 $^{\text{th}}$ order and reduced second-order system for Case 1 is depicted in Figure 20. Similarly, the reduced order transfer function for Case 2 to Case 4 can be obtained and is expressed as follows,

$$\text{CLTF}_{(\text{case}-2)} = \frac{-0.01447s^2 - 5.864s + 1.989 \times 10^{-11}}{s^2 + 23.15s + 141} \tag{68}$$

$$\text{CLTF}_{(\text{case}-3)} = \frac{-0.08989s^2 - 1.696s + 1.38 \times 10^{-12}}{s^2 + 4.75s + 35.99}) \tag{69}$$

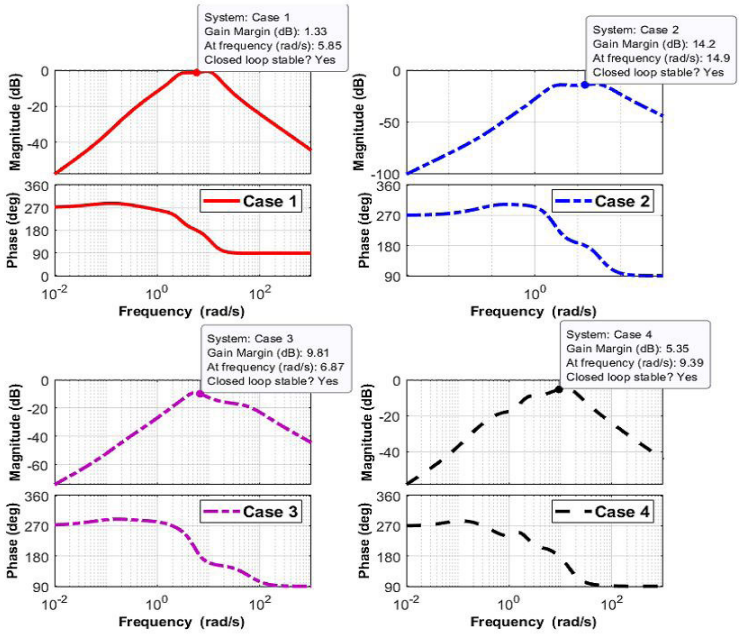

FIGURE 21. Frequency response of reduced order system using PSO-GSA tuned cascade PI-PD controller.

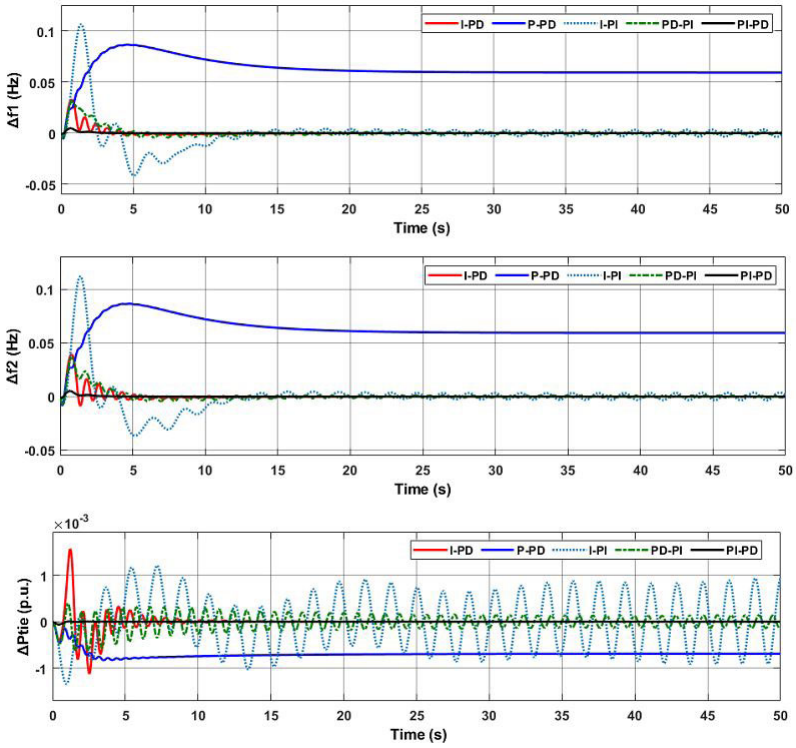

FIGURE 22. Performance comparisons of various cascade controllers for two-area HPS.

$$\mathrm{CLTF}_{(\mathrm{case}-4)} = \frac{0.1109s^2 - 11.74s + 1.901 \times 10^{-11}}{s^2 + 22.74s + 82.29} \tag{70}$$

Figure 21 represents the frequency analysis of various cases that has different generating units to balance the load and thereby maintaining the system frequency and tie-line

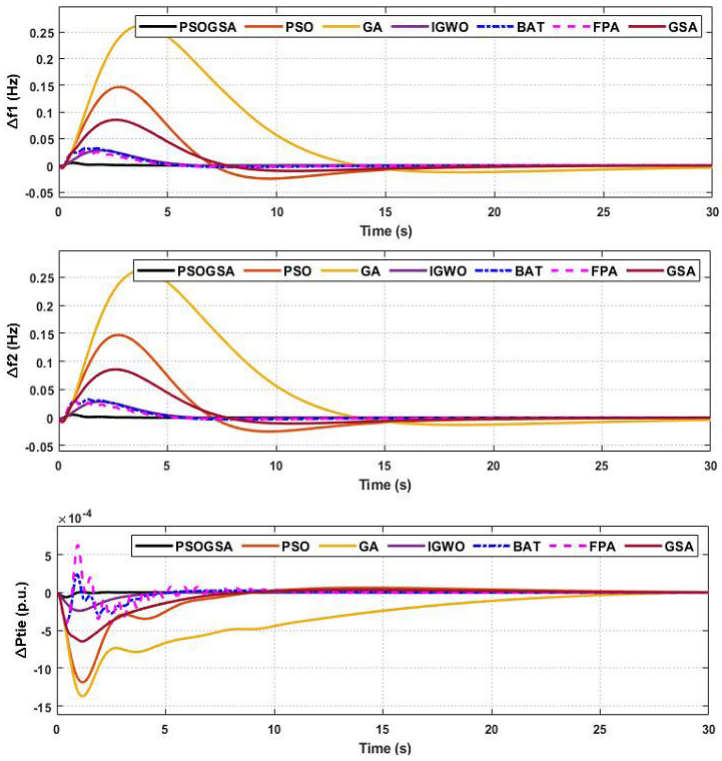

FIGURE 23. Performance comparisons of various intelligence methods for two-area HPS.

power within the tolerable limits. The bode analysis of various cases shows the system was stable for the tuned gain values of controller using the presented PSO-GSA method.

VII. COMPARATIVE ANALYSIS

This section presents the comparative analysis of the proposed cascade controller with other combination of cascade control and also with the recent literature in the forthcoming subsections.

A. COMPARISON OF DIFFERENT CCs FOR HPS

To further validate the proposed PI-PD control as the best choice for HPS model, this section compares the proffered controller with other combination of CCs such as I-PD, P-PD, I-PI, and PD-PI. To study this, Case 3 was considered for the analysis and the tuned gain values for various controller using PSO-GSA method are: I-PD ($K_i = -4$, $K_p = 2.9139$, $K_d = 0.9355$) P-PD ($K_p = -1$, $K_{p1} = 1$, $K_d = 0.9659$), I-PI ($K_i = -0.9764$, $K_p = 0.9005$, $K_{i1} = 0.5177$) and PD-PI ($K_p = -1.1878$, $K_d = -1.3847$, $K_{p1} = 1.1404$, $K_i = 1.9958$), respectively. The dynamic response for the various combinations of CCs is portrayed in Figure 22. The result shows that the integral combination of cascade controllers settled at zero steady state error except the I-PI controller, whose response oscillated with minimum value of steady state error. On the other hand, the P-PD controller settled with steady state error value of 0.06. Among the various scheme presented, I-PD and PI-PD combination performed better. However, the I-PD controller also suffered from initial oscillation in the response and their settling time was higher than that of the PI-PD. Therefore, this work claims that the PI-PD is the best choice of cascade control for HPS operation with the integration of various types of power generation.

B. COMPARISON OF PI-PD CONTROL WITH LITERATURE WORK

To prove the efficiency of the method, the two-area HPS model presented in Case 3 was considered for a comparative analysis with the literature work. The performance of PSO-GSA tuned cascade PI-PD controller outperformed the recent research work presented in the literature such as GA, PSO, GSA, Bat, FPA, and IGWO. The gain values of various intelligence methods are obtained by minimizing the IAE criterion. It is inferred from Figure 23 that the frequency and tie-line power variation settle faster with minimum overshoot by the suggested method compared to other AI techniques presented.

VIII. CONCLUSION

In this work, a PSO-GSA tuned cascade PI-PD control for ALFC of diverse units with multisource power generation of both conventional and RE system was addressed. Initially, the performance of cascade PI-PD was compared with other classical controllers such as I, PI, PID, and IPD control for system with various cases: Case 1 (thermal source), Case 2

(thermal, hydro, and gas), Case 3 (thermal, RE), and Case 4 [unequal area: area 1 (thermal, hydro and gas), area 2: (thermal and renewable energy)]. The results for various cases show that the cascade PI-PD control gives significant reduction of almost 20% to 70% in settling time, rise time, and peak time, 5% to 92% in peak over/undershoots, 10% to 90% in peak magnitude and control effort of transient performance indices. Similarly, the steady state indices such as IAE, ITAE, ISE, and ITSE were also reduced by 10% to 95% for various disparate cases of power system operation than those of the other classical controllers. The robustness of the controller was also validated for simultaneous change in wind power and load variation. The over/undershoot of frequency and tie-line power deviations were considerably reduced for the proposed controller. Furthermore, the efficiency of optimized gain values of controller at nominal loading was tested for the change in system parameters and conditions such as SLP, inertia constant and system loading. The sensitivity analysis also reveals that the gain values obtained were robust for a wide change in the system parameters and retuning is not required. The results obtained were compared with literature results of AI methods such as GA, PSO, GSA, Bat, FPA, and IGWO techniques. The outcome demonstrates that the system performance is better for the suggested PSO-GSA based meta-heuristic optimization method. Furthermore, the Hankel form of model order reduction technique through the state space approach was used to reduce the higher order (13^{th} order) model to second-order transfer function for stability analysis of the system. The stability study of various cases using bode analysis reveals that the tuned gain values of cascade PI-PD controller is appropriate for stable operation of system with minimum control efforts. The analysis of multi-area HPS model with self-adaptive controllers in the presence of FACTS device, HVDC link, and electric vehicles will be the future goal of research.

APPENDIXES

APPENDIX I

Case 1 (Thermal): Area (A) capacity of 2000 MW, Frequency $f = 60$ Hz, Power system gain and Time constant: $K_{P1} = K_{P2} = 120$ Hz/p.u.MW, $T_{P1} = T_{P2} = 20$ s, Governor Time constant: $T_{G1} = T_{G2} = 0.08$ s, Time constant of turbine: $T_{T1} = T_{T2} = 0.3$ s,Time and gain constant of Reheat: $T_{r1} = T_{r2} = 10$ s and $K_{r1} = K_{r2} = 0.2$, Droop constant: $R_1 = R_2 = 2.4$ Hz/p.u.MW, Frequency Bias constant: $B_1 = B_2 = 0.425$ p.u.MW/Hz, Inertia $H_1 = H_2 = 5$ s, Tie-line coefficients: $T_{12} = T_{21} = 0.08674$ p.u.MW/rad, Per units of area capacity: $D_1 = D_2 = 0.00833$ p.u.MW/rad, governor dead band (GDB) = 0.05% governor rate constraints (GRC) = 3% [43].

Case 2 (Multi-Source): In this case, the two-area model consists of of thermal, hydro and gas power generation. Thermal - the simulation parameters are same like case 1. Hydro turbine model parameters - $T_H = 28.75$ s, $T_{\text{RS}} = 1$ s, $T_{\text{RH}} = 0.3$, $T_w = 3.06$ s, $K_H = 0.5747$, Gas Turbine model parameters - $C_g = 1$, $b_g = 0.05$ s, $X_c = 0.6$ s, $Y_c = 1$ s, $T_{\text{CR}} = 0.01$ s, $T_F = 0.23$ s, $T_{\text{CD}} = 0.2$ s, $K_G = 0.1304$, HVDC link gain and time constant - $K_{\text{dc}} = 1$, $T_{\text{dc}} = 0.2$ s, Power System gain and time constant: $K_{p1} = K_{p2} = 68.9566$ and $T_{p1} = T_{p2} = 11.49$ s.

$$X = \begin{bmatrix} \Delta f_1 & \Delta f_2 & \Delta P_{c1} & \Delta P_{c2} & \Delta P_{T1} & \Delta P_{T2} & \Delta T_{T1} & \Delta T_{T2} & \Delta G_{T1} & \Delta G_{T2} & \Delta P_{g1} & \Delta P_{g2} & \Delta P_{\text{tie},1} \end{bmatrix}^T \tag{73}$$

$$A = \begin{bmatrix} -0.05 & 0 & -0.44 & 0 & 0 & 1 & 0 & 0 & 0 & 0 & 0 & 0 & 0 \\ 0 & -0.05 & 0.44 & 0 & 0 & 0 & 0 & 0 & 1 & 0 & 0 & 0 & 0 \\ 6 & -6 & 0 & 0 & 0 & 0 & 0 & 0 & 0 & 0 & 0 & 0 & 0 \\ -646.47 & 0 & 10.24 & -12.5 & 0 & 0 & 0 & 0 & 0 & 282.1 & -80 & 0 & 0 \\ 0 & 0 & 0 & 12.5 & -0.1 & 0 & 0 & 0 & 0 & 0 & 0 & 0 & 0 \\ 0 & 0 & 0 & 20.83 & 0.17 & -3.33 & 0 & 0 & 0 & 0 & 0 & 0 & 0 \\ 0 & -646.47 & -10.24 & 0 & 0 & 0 & -12.5 & 0 & 0 & 0 & 0 & 282.1 & -80 \\ 0 & 0 & 0 & 0 & 0 & 0 & 12.5 & -0.1 & 0 & 0 & 0 & 0 & 0 \\ 0 & 0 & 0 & 0 & 0 & 0 & 20.83 & 0.17 & -3.33 & 0 & 0 & 0 & 0 \\ -5.77 & 0 & -1.01 & 0 & 0 & 0 & 0 & 0 & 0 & 0 & 0 & 0 & 0 \\ -796.64 & 0 & 12.62 & 0 & 0 & 0 & 0 & 0 & 0 & 347.62 & -100 & 0 & 0 \\ 0 & -5.77 & 1.01 & 0 & 0 & 0 & 0 & 0 & 0 & 0 & 0 & 0 & 0 \\ 0 & -796.64 & -12.62 & 0 & 0 & 0 & 0 & 0 & 0 & 0 & 0 & 347.62 & -100 \end{bmatrix} \tag{74}$$

$$B = \begin{bmatrix} 0 & 0 & 0.1 & 0 & 0 & 0 & 0 & 0 & 0 & 0 & 0 & 0 & 0 \\ 0 & 0 & 0 & 12.5 & 0 & 0 & 0 & 0 & 0 & 0 & 0 & 0 & 0 \end{bmatrix}^T \tag{75}$$

$$C = \begin{bmatrix} 1 & 1 & 0 & 0 & 0 & 0 & 0 & 0 & 0 & 0 & 0 & 0 & 1 \end{bmatrix}^T \tag{76}$$

Case 3 (Thermal HPS): In this case, the thermal model is integrated with RE sources and the details are: Thermal model - As similar to case 1, RE source Model- Wind turbine gain and time constant: $K_{WTG} = 1$, $T_{WTG} = 1.5$ s, DEG gain and time constant:$K_{DEG} = 0.0033$, $T_{DEG} = 2$ s, AE gain and time constant: $K_{AE} = 0.002$, $T_{AE} = 0.5$ s, FC gain and time constant: $K_{FC} = 0.01$, $T_{FC} = 4$ s, BESS gain and time constant: $K_{BESS} = -0.0033$, $T_{BESS} = 0.1$ s [46].

Case 4 (Multi-Source HPS): Area 1 consists of Thermal, Hydro and Gas power generation and their details are given in case 2. Area 2 is a thermal system integrated with RE source and their parameters for simulations are same as case 3.

APPENDIX II

The numerator and denominator of CLTF of case-1 given in (58) can be represented as,

$$\begin{aligned}\text{num} = &-6s^{12} - 1392s^{11} - (1.004 \times 10^5)s^{10} \\ &-(2.418 \times 10^6)s^9 - (3.218 \times 10^7)s^8 \\ &-(2.636 \times 10^8)s^7 - (1.132 \times 10^9)s^6\end{aligned}$$

$$H_1^{(0)} = \begin{bmatrix} 8.61 \times 10^{-17} & -6.0 \times 10^{00} & 3.0 \times 10^{-01} & 1.59 \times 10^{01} & 8.08 \times 10^{04} & -9.05 \times 10^{06} & 9.17 \times 10^{08} \\ -6.00 \times 10^{00} & 3.0 \times 10^{-01} & 1.59 \times 10^{01} & 8.08 \times 10^{04} & -9.05 \times 10^{06} & 9.17 \times 10^{08} & -9.29 \times 10^{10} \\ 3.00 \times 10^{-01} & 1.59 \times 10^{01} & 8.08 \times 10^{04} & -9.05 \times 10^{06} & 9.17 \times 10^{08} & -9.29 \times 10^{10} & 9.43 \times 10^{12} \\ 1.59 \times 10^{01} & 8.08 \times 10^{04} & -9.05 \times 10^{06} & 9.17 \times 10^{08} & -9.29 \times 10^{10} & 9.43 \times 10^{12} & -9.57 \times 10^{14} \\ 8.08 \times 10^{04} & -9.05 \times 10^{06} & 9.17 \times 10^{08} & -9.29 \times 10^{10} & 9.43 \times 10^{12} & -9.57 \times 10^{14} & 9.71 \times 10^{16} \\ -9.05 \times 10^{06} & 9.1704 \times 10^{08} & -9.29 \times 10^{10} & 9.43 \times 10^{12} & -9.57 \times 10^{14} & 9.71 \times 10^{16} & -9.85 \times 10^{18} \\ 9.17 \times 10^{08} & -9.29 \times 10^{10} & 9.43 \times 10^{12} & -9.57 \times 10^{14} & 9.71 \times 10^{16} & -9.85 \times 10^{18} & 1.00 \times 10^{21} \\ -9.29 \times 10^{10} & 9.43 \times 10^{12} & -9.57 \times 10^{14} & 9.71 \times 10^{16} & -9.85 \times 10^{18} & 1.00 \times 10^{21} & -1.01 \times 10^{23} \\ 9.43 \times 10^{12} & -9.57 \times 10^{14} & 9.71 \times 10^{16} & -9.85 \times 10^{18} & 1.00 \times 10^{21} & -1.01 \times 10^{23} & 1.03 \times 10^{25} \\ -9.57 \times 10^{14} & 9.71 \times 10^{16} & -9.85 \times 10^{18} & 1.00 \times 10^{21} & -1.01 \times 10^{23} & 1.03 \times 10^{25} & -1.04 \times 10^{27} \\ 9.71 \times 10^{16} & -9.85 \times 10^{18} & 1.00 \times 10^{21} & -1.01 \times 10^{23} & 1.03 \times 10^{25} & -1.04 \times 10^{27} & 1.06 \times 10^{29} \\ -9.85 \times 10^{18} & 1.00 \times 10^{21} & -1.01 \times 10^{23} & 1.03 \times 10^{25} & -1.04 \times 10^{27} & 1.06 \times 10^{29} & -1.07 \times 10^{31} \\ 1.00 \times 10^{21} & -1.01 \times 10^{23} & 1.03 \times 10^{25} & -1.04 \times 10^{27} & 1.06 \times 10^{29} & -1.07 \times 10^{31} & 1.09 \times 10^{33} \end{bmatrix} \tag{77}$$

$$H_2^{(0)} = \begin{bmatrix} -9.29 \times 10^{10} & 9.43 \times 10^{12} & -9.57 \times 10^{14} & 9.71 \times 10^{16} & -9.85 \times 10^{18} & 1.00 \times 10^{21} \\ 9.43 \times 10^{12} & -9.57 \times 10^{14} & 9.71 \times 10^{16} & -9.85 \times 10^{18} & 1.00 \times 10^{21} & -1.01 \times 10^{23} \\ -9.57 \times 10^{14} & 9.71 \times 10^{16} & -9.85 \times 10^{18} & 1.00 \times 10^{21} & -1.01 \times 10^{23} & 1.03 \times 10^{25} \\ 9.71 \times 10^{16} & -9.85 \times 10^{18} & 1.00 \times 10^{21} & -1.01 \times 10^{23} & 1.03 \times 10^{25} & -1.04 \times 10^{27} \\ -9.85 \times 10^{18} & 1.00 \times 10^{21} & -1.01 \times 10^{23} & 1.03 \times 10^{25} & -1.04 \times 10^{27} & 1.06 \times 10^{29} \\ 1.00 \times 10^{21} & -1.01 \times 10^{23} & 1.03 \times 10^{25} & -1.04 \times 10^{27} & 1.06 \times 10^{29} & -1.07 \times 10^{31} \\ -1.01 \times 10^{23} & 1.03 \times 10^{25} & -1.04 \times 10^{27} & 1.06 \times 10^{29} & -1.07 \times 10^{31} & 1.09 \times 10^{33} \\ 1.03 \times 10^{25} & -1.04 \times 10^{27} & 1.06 \times 10^{29} & -1.07 \times 10^{31} & 1.09 \times 10^{33} & -1.10 \times 10^{35} \\ -1.04 \times 10^{27} & 1.06 \times 10^{29} & -1.07 \times 10^{31} & 1.09 \times 10^{33} & -1.10 \times 10^{35} & 1.12 \times 10^{37} \\ 1.06 \times 10^{29} & -1.07 \times 10^{31} & 1.09 \times 10^{33} & -1.10 \times 10^{35} & 1.12 \times 10^{37} & -1.14 \times 10^{39} \\ -1.07 \times 10^{31} & 1.09 \times 10^{33} & -1.10 \times 10^{35} & 1.12 \times 10^{37} & -1.14 \times 10^{39} & 1.15 \times 10^{41} \\ 1.09 \times 10^{33} & -1.10 \times 10^{35} & 1.12 \times 10^{37} & -1.14 \times 10^{39} & 1.159 \times 10^{41} & -1.17 \times 10^{43} \\ -1.10 \times 10^{35} & 1.12 \times 10^{37} & -1.14 \times 10^{39} & 1.15 \times 10^{41} & -1.17 \times 10^{43} & 1.193 \times 10^{45} \end{bmatrix} \tag{78}$$

$$H_3^{(1)} = \begin{bmatrix} 1 & -6.96 \times 10^{16} & 3.48 \times 10^{15} & 1.85 \times 10^{17} & 9.37 \times 10^{20} & -1.05 \times 10^{23} & 1.06 \times 10^{25} \\ 0 & -4.17 \times 10^{17} & 2.08 \times 10^{16} & 1.11 \times 10^{18} & 5.62 \times 10^{21} & -6.30 \times 10^{23} & 6.38 \times 10^{25} \\ 0 & 2.08 \times 10^{16} & -1.04 \times 10^{15} & -5.56 \times 10^{16} & -2.81 \times 10^{20} & 3.15 \times 10^{22} & -3.19 \times 10^{24} \\ 0 & 1.11 \times 10^{18} & -5.56 \times 10^{16} & -2.96 \times 10^{18} & -1.49 \times 10^{22} & 1.67 \times 10^{24} & -1.70 \times 10^{26} \\ 0 & 5.62 \times 10^{21} & -2.81 \times 10^{20} & -1.49 \times 10^{22} & -7.57 \times 10^{25} & 8.48 \times 10^{27} & -8.59 \times 10^{29} \\ 0 & -6.30 \times 10^{23} & 3.15 \times 10^{22} & 1.67 \times 10^{24} & 8.48 \times 10^{27} & -9.50 \times 10^{29} & 9.62 \times 10^{31} \\ 0 & 6.38 \times 10^{25} & -3.19 \times 10^{24} & -1.70 \times 10^{26} & -8.59 \times 10^{29} & 9.62 \times 10^{31} & -9.75 \times 10^{33} \\ 0 & -6.47 \times 10^{27} & 3.23 \times 10^{26} & 1.72 \times 10^{28} & 8.71 \times 10^{31} & -9.75 \times 10^{33} & 9.88 \times 10^{35} \\ 0 & 6.56 \times 10^{29} & -3.28 \times 10^{28} & -1.74 \times 10^{30} & -8.84 \times 10^{33} & 9.90 \times 10^{35} & -1.00 \times 10^{38} \\ 0 & -6.66 \times 10^{31} & 3.33 \times 10^{30} & 1.77 \times 10^{32} & 8.97 \times 10^{35} & 1.00 \times 10^{38} & 1.01 \times 10^{40} \\ 0 & 6.76 \times 10^{33} & -3.38 \times 10^{32} & -1.80 \times 10^{34} & 9.10 \times 10^{37} & 1.01 \times 10^{40} & 1.03 \times 10^{42} \\ 0 & -6.86 \times 10^{35} & 3.43 \times 10^{34} & 1.82 \times 10^{36} & 9.24 \times 10^{39} & -1.03 \times 10^{42} & -1.04 \times 10^{44} \\ 0 & 6.96 \times 10^{37} & -3.48 \times 10^{36} & -1.85 \times 10^{38} & -9.37 \times 10^{41} & -1.05 \times 10^{44} & 1.06 \times 10^{46} \end{bmatrix} \tag{79}$$

$$
\begin{aligned}
&-(2.653\times10^{9})s^{5}-(3.511\times10^{9})s^{4}\\
&-(2.116\times10^{9})s^{3}-(4.302\times10^{8})s^{2}\\
&-(2.512\times10^{7})s \qquad (71)\\
\text{den} = {}& s^{13}+232s^{12}+\left(1.674\times10^{4}\right)s^{11}\\
&+\left(4.18\times10^{5}\right)s^{10}+\left(7.044\times10^{6}\right)s^{9}\\
&+(7.383\times10^{7})s^{8}+\left(5.503\times10^{8}\right)s^{7}\\
&+\left(2.516\times10^{9}\right)s^{6}+\left(7.486\times10^{9}\right)s^{5}\\
&+\left(1.449\times10^{10}\right)s^{4}+\left(1.676\times10^{10}\right)s^{3}\\
&+\left(9.94\times10^{9}\right)s^{2}+\left(2.388\times10^{9}\right)s\\
&+\left(1.932\times10^{8}\right) \qquad (72)
\end{aligned}
$$

The state vector of thermal system (case-1) is defined as, (73) shown at the bottom of the 20th page.

For the above state vector, the state space input and output matrices of CLTF defined in (58) are represented as (74)–(76) shown at the bottom of the 20th page.

$$
H_4^{(1)} = \begin{bmatrix}
-1.07\times10^{27} & 1.09\times10^{29} & -1.11\times10^{31} & 1.12\times10^{33} & -1.14\times10^{35} & 1.16\times10^{37}\\
-6.47\times10^{27} & 6.56\times10^{29} & -6.66\times10^{31} & 6.76\times10^{33} & -6.86\times10^{35} & 6.96\times10^{37}\\
3.23\times10^{26} & -3.28\times10^{28} & 3.33\times10^{30} & -3.38\times10^{32} & 3.43\times10^{34} & -3.48\times10^{36}\\
1.72\times10^{28} & -1.74\times10^{30} & 1.77\times10^{32} & -1.80\times10^{34} & 1.82\times10^{36} & -1.85\times10^{38}\\
8.71\times10^{31} & -8.84\times10^{33} & 8.97\times10^{35} & -9.10\times10^{37} & 9.24\times10^{39} & -9.37\times10^{41}\\
-9.75\times10^{33} & 9.90\times10^{35} & -1.00\times10^{38} & 1.01\times10^{40} & -1.03\times10^{42} & 1.05\times10^{44}\\
9.88\times10^{35} & -1.00\times10^{38} & 1.01\times10^{40} & -1.03\times10^{42} & 1.04\times10^{44} & -1.06\times10^{46}\\
-1.00\times10^{38} & 1.01\times10^{40} & -1.03\times10^{42} & 1.04\times10^{44} & -1.06\times10^{46} & 1.07\times10^{48}\\
1.01\times10^{40} & -1.03\times10^{42} & 1.04\times10^{44} & -1.06\times10^{46} & 1.07\times10^{48} & -1.09\times10^{50}\\
1.03\times10^{42} & 1.04\times10^{44} & -1.06\times10^{46} & 1.07\times10^{48} & 1.09\times10^{50} & 1.10\times10^{52}\\
1.04\times10^{44} & -1.06\times10^{46} & -1.07\times10^{48} & -1.09\times10^{50} & -1.10\times10^{52} & -1.12\times10^{54}\\
1.06\times10^{46} & 1.07\times10^{48} & 1.09\times10^{50} & 1.10\times10^{52} & 1.12\times10^{54} & -1.14\times10^{56}\\
1.07\times10^{48} & -1.09\times10^{50} & -1.10\times10^{52} & -1.12\times10^{54} & -1.14\times10^{56} & 1.15\times10^{58}
\end{bmatrix} \qquad (80)
$$

$$
H_5^{(2)} = \begin{bmatrix}
1 & 0 & -2.50 & -1.35\times10^{04} & 1.57\times10^{06} & -1.34\times10^{08} & 1.28\times10^{10}\\
0 & 1 & 0 & 0 & 0 & 0 & 0\\
0 & 0 & 8.08\times10^{04} & -9.04\times10^{06} & 9.16\times10^{08} & -9.29\times10^{10} & 9.42\times10^{12}\\
0 & 0 & -9.04\times10^{06} & 9.17\times10^{08} & -9.18\times10^{10} & 9.31\times10^{12} & -9.45\times10^{14}\\
0 & 0 & 9.16\times10^{08} & -9.18\times10^{10} & 9.18\times10^{12} & -9.32\times10^{14} & 9.44\times10^{16}\\
0 & 0 & -9.29\times10^{10} & 9.31\times10^{12} & -9.30\times10^{14} & 9.44\times10^{16} & -9.58\times10^{18}\\
0 & 0 & 9.42\times10^{12} & -9.45\times10^{14} & 9.42\times10^{16} & -9.56\times10^{18} & 9.73\times10^{20}\\
0 & 0 & -9.56\times10^{14} & 9.59\times10^{16} & -9.58\times10^{18} & 9.73\times10^{20} & -9.87\times10^{22}\\
0 & 0 & 9.71\times10^{16} & -9.73\times10^{18} & 9.73\times10^{20} & -9.87\times10^{22} & 9.99\times10^{24}\\
0 & 0 & -9.85\times10^{18} & 9.87\times10^{20} & -9.87\times10^{22} & 1.00\times10^{25} & -1.01\times10^{27}\\
0 & 0 & 1.00\times10^{21} & -1.00\times10^{23} & 9.99\times10^{24} & -1.01\times10^{27} & 1.03\times10^{29}\\
0 & 0 & -1.01\times10^{23} & 1.01\times10^{25} & -1.01\times10^{27} & 1.03\times10^{29} & -1.04\times10^{31}\\
0 & 0 & 1.02\times10^{25} & -1.03\times10^{27} & 1.03\times10^{29} & -1.04\times10^{31} & 1.06\times10^{33}
\end{bmatrix} \qquad (81)
$$

$$
H_6^{(2)} = \begin{bmatrix}
-1.51\times10^{12} & 1.58\times10^{14} & -1.35\times10^{16} & 1.58\times10^{18} & -1.66\times10^{20} & 1.41\times10^{22}\\
0 & 0 & 0 & 0 & 0 & 0\\
-9.56\times10^{14} & 9.71\times10^{16} & -9.85\times10^{18} & 1.00\times10^{21} & -1.01\times10^{23} & 1.03\times10^{25}\\
9.59\times10^{16} & -9.73\times10^{18} & 9.87\times10^{20} & -1.00\times10^{23} & 1.01\times10^{25} & -1.03\times10^{27}\\
-9.58\times10^{18} & 9.73\times10^{20} & -9.87\times10^{22} & 1.00\times10^{25} & -1.01\times10^{27} & 1.03\times10^{29}\\
9.71\times10^{20} & -9.85\times10^{22} & 1.00\times10^{25} & -1.01\times10^{27} & 1.02\times10^{29} & -1.04\times10^{31}\\
-9.85\times10^{22} & 9.99\times10^{24} & -1.01\times10^{27} & 1.03\times10^{29} & -1.04\times10^{31} & 1.06\times10^{33}\\
9.99\times10^{24} & -1.01\times10^{27} & 1.03\times10^{29} & -1.04\times10^{31} & 1.05\times10^{33} & -1.07\times10^{35}\\
-1.01\times10^{27} & 1.03\times10^{29} & -1.04\times10^{31} & 1.06\times10^{33} & -1.07\times10^{35} & 1.09\times10^{37}\\
1.03\times10^{29} & -1.04\times10^{31} & 1.06\times10^{33} & -1.07\times10^{35} & 1.09\times10^{37} & -1.10\times10^{39}\\
-1.04\times10^{31} & 1.05\times10^{33} & -1.07\times10^{35} & 1.09\times10^{37} & -1.10\times10^{39} & 1.12\times10^{41}\\
1.05\times10^{33} & -1.07\times10^{35} & 1.09\times10^{37} & -1.10\times10^{39} & 1.121\times0^{41} & -1.14\times10^{43}\\
-1.07\times10^{35} & 1.09\times10^{37} & -1.10\times10^{39} & 1.12\times10^{41} & -1.14\times10^{43} & 1.15\times10^{45}
\end{bmatrix} \qquad (82)
$$

The sub-matrices of Hankel matrix $H_{1313}^{(0)}$ in Hermite form is defined as follows (77) and (78) shown at the bottom of the 21th page.

The sub-matrices of Hankel matrix $H_{1313}^{(1)}$ in Hermite form is defined as follows (79) and (81) shown at the bottom of the 22th page.

The sub-matrices of Hankel matrix $H_{1313}^{(2)}$ in Hermite form is defined as follows (82) and (83) shown at the bottom of the 22th page.

REFERENCES

[1] O. I. Elgerd, *Electric Energy Systems Theory: An Introduction*. New York, NY, USA: McGraw-Hill, 1976.
[2] B. Pal and B. Chaudhuri, *Robust Control in Power Systems*, 1st ed. New York, NY, USA: Springer, 2005.
[3] H. Bevrani, A. Ghosh, and G. Ledwich, "Renewable energy sources and frequency regulation: Survey and new perspectives," *IET Renew. Power Gener.*, vol. 4, no. 5, pp. 438–457, Sep. 2010.
[4] D. Qian and G. Fan, "Neural-network-based terminal sliding mode control for frequency stabilization of renewable power systems," *IEEE/CAA J. Autom. Sinica*, vol. 5, no. 3, pp. 706–717, May 2018.
[5] K. Liao and Y. Xu, "A robust load frequency control scheme for power systems based on second-order sliding mode and extended disturbance observer," *IEEE Trans. Ind. Informat.*, vol. 14, no. 7, pp. 3076–3086, Jul. 2018.
[6] H. Zhang, J. Liu, and S. Xu, "H-infinity load frequency control of networked power systems via an event-triggered scheme," *IEEE Trans. Ind. Electron.*, vol. 67, no. 8, pp. 7104–7113, Aug. 2020, doi: 10.1109/TIE.2019.2939994.
[7] S. Kayalvizhi and D. M. V. Kumar, "Load frequency control of an isolated micro grid using fuzzy adaptive model predictive control," *IEEE Access*, vol. 5, pp. 16241–16251, 2017.
[8] M.-H. Khooban, "Secondary load frequency control of time-delay stand-alone microgrids with electric vehicles," *IEEE Trans. Ind. Electron.*, vol. 65, no. 9, pp. 7416–7422, Sep. 2018.
[9] R. K. Sahu, S. Panda, A. Biswal, and G. T. C. Sekhar, "Design and analysis of tilt integral derivative controller with filter for load frequency control of multi-area interconnected power systems," *ISA Trans.*, vol. 61, pp. 251–264, Mar. 2016.
[10] D. Saha and L. C. Saikia, "Automatic generation control of a multi-area CCGT-thermal power system using stochastic search optimised integral minus proportional derivative controller under restructured environment," *IET Gener., Transmiss. Distrib.*, vol. 11, no. 15, pp. 3801–3813, Oct. 2017.
[11] J. G. Ziegler and N. B. Nichols, "Optimum settings for automatic controllers," *Trans. Amer. Soc. Mech. Eng.*, vol. 64, pp. 759–765, Nov. 1942.
[12] H. A. Yousef, *Power System Load Frequency Control: Classical and Adaptive Fuzzy Approaches*, 1st ed. New York, NY, USA: Taylor & Francis, 2017.
[13] H. M. Hasanien and S. M. Muyeen, "A taguchi approach for optimum design of proportional-integral controllers in cascaded control scheme," *IEEE Trans. Power Syst.*, vol. 28, no. 2, pp. 1636–1644, May 2013.
[14] C. Wang, J. Li, and Y. Hu, "Frequency control of isolated wind-diesel microgrid power system by double equivalent-input-disturbance controllers," *IEEE Access*, vol. 7, pp. 105617–105626, 2019.
[15] S. Sumathi, L. A. Kumar, and P. Surekha, *Computational Intelligence Paradigms for Optimization Problems using MATLAB/SIMULINK*. New York, NY, USA: Taylor & Francis, 2016.
[16] Y. Arya, "Impact of hydrogen Aqua electrolyzer-fuel cell units on automatic generation control of power systems with a new optimal fuzzy TIDF-II controller," *Renew. Energy*, vol. 139, pp. 468–482, Aug. 2019.
[17] S. Aziz, H. Wang, Y. Liu, J. Peng, and H. Jiang, "Variable universe fuzzy logic-based hybrid LFC control with real-time implementation," *IEEE Access*, vol. 7, pp. 25535–25546, 2019.
[18] F. Beaufays, Y. Abdel-Magid, and B. Widrow, "Application of neural networks to load-frequency control in power systems," *Neural Netw.*, vol. 7, no. 1, pp. 183–194, Jan. 1994.
[19] R. Ramachandran, B. Madasamy, V. Veerasamy, and L. Saravanan, "Load frequency control of a dynamic interconnected power system using generalised hopfield neural network based self-adaptive PID controller," *IET Gener., Transmiss. Distrib.*, vol. 12, no. 21, pp. 5713–5722, Nov. 2018.
[20] D. C. Das, A. Roy, and N. Sinha, "GA based frequency controller for solar thermal–diesel–wind hybrid energy generation/energy storage system," *Int. J. Elect. Power Energy Syst.*, vol. 43, no. 1, pp. 262–279, 2012.
[21] H. Gozde and M. C. Taplamacioglu, "Automatic generation control application with craziness based particle swarm optimization in a thermal power system," *Int. J. Elect. Power Energy Syst.*, vol. 33, no. 1, pp. 8–16, Jan. 2011.
[22] A. K. Barisal, "Comparative performance analysis of teaching learning based optimization for automatic load frequency control of multi-source power systems," *Int. J. Elect. Power Energy Syst.*, vol. 66, pp. 67–77, Mar. 2015.
[23] M. Gheisarnejad, "An effective hybrid harmony search and cuckoo optimization algorithm based fuzzy PID controller for load frequency control," *Appl. Soft Comput.*, vol. 65, pp. 121–138, Apr. 2018.
[24] M. W. Iruthayarajan and S. Baskar, "Evolutionary algorithms based design of multivariable PID controller," *Expert Syst. Appl.*, vol. 36, no. 5, pp. 9159–9167, Jul. 2009.
[25] A. K. Barik and D. C. Das, "Proficient load-frequency regulation of demand response supported bio-renewable cogeneration based hybrid microgrids with quasi-oppositional selfish-herd optimisation," *IET Gener., Transmiss. Distrib.*, vol. 13, no. 13, pp. 2889–2898, Jul. 2019.
[26] D. Saha and L. C. Saikia, "Automatic generation control of an interconnected CCGT-thermal system using stochastic fractal search optimized classical controllers," *Int. Trans. Electr. Energy Syst.*, vol. 28, no. 5, p. e2533, May 2018.
[27] A. K. Barik and D. C. Das, "Coordinated regulation of voltage and load frequency in demand response supported biorenewable cogeneration-based isolated hybrid microgrid with quasi-oppositional selfish herd optimisation," *Int. Trans. Electr. Energy Syst.*, vol. 30, no. 1, 2020, Art. no. e12176.
[28] K. Ogata and Y. Yang, *Modern Control Engineering*, vol. 17, 5th ed. Upper Saddle River, NJ, USA: Pearson, 2010.
[29] P. R. Krishnaswamy, G. P. Rangaiah, R. K. Jha, and P. B. Deshpande, "When to use cascade control," *Ind. Eng. Chem. Res.*, vol. 29, no. 10, pp. 2163–2166, Oct. 1990.
[30] İ. Kaya, N. Tan, and D. P. Atherton, "Improved cascade control structure for enhanced performance," *J. Process Control*, vol. 17, no. 1, pp. 3–16, Jan. 2007.
[31] P. Dash, L. C. Saikia, and N. Sinha, "Flower pollination algorithm optimized PI-PD cascade controller in automatic generation control of a multi-area power system," *Int. J. Elect. Power Energy Syst.*, vol. 82, pp. 19–28, Nov. 2016.
[32] M. Gheisarnejad and M. H. Khooban, "Secondary load frequency control for multi-microgrids: HiL real-time simulation," *Soft Comput.*, vol. 23, no. 14, pp. 5785–5798, Jul. 2019.
[33] S. Padhy and S. Panda, "A hybrid stochastic fractal search and pattern search technique based cascade PI-PD controller for automatic generation control of multi-source power systems in presence of plug in electric vehicles," *CAAI Trans. Intell. Technol.*, vol. 2, no. 1, pp. 12–25, Mar. 2017.
[34] L. C. Saikia and D. Saha, "Automatic generation control in competitive market conditions with moth-flame optimization based cascade controller," in *Proc. IEEE Reg. Annu. Int. Conf. (TENCON)*, Nov. 2017, pp. 734–738.
[35] S. Padhy, S. Panda, and S. Mahapatra, "A modified GWO technique based cascade PI-PD controller for AGC of power systems in presence of plug in electric vehicles," *Eng. Sci. Technol., Int. J.*, vol. 20, no. 2, pp. 427–442, Apr. 2017.
[36] C. C. Hang, A. P. Loh, and V. U. Vasnani, "Relay feedback auto-tuning of cascade controllers," *IEEE Trans. Control Syst. Technol.*, vol. 2, no. 1, pp. 42–45, Mar. 1994.
[37] I. Kaya, "Improving performance using cascade control and a smith predictor," *ISA Trans.*, vol. 40, no. 3, pp. 223–234, Jul. 2001.
[38] W. Tan, J. Liu, T. Chen, and H. J. Marquez, "Robust analysis and PID tuning of cascade control systems," *Chem. Eng. Commun.*, vol. 192, no. 9, pp. 1204–1220, Sep. 2005.
[39] C. C. Yu and W. L. Luyben, "Conditional stability in cascade control," *Ind. Eng. Chem. Fundam.*, vol. 25, no. 1, pp. 171–174, Feb. 1986.
[40] M. Thirumeni and D. Thangavelusamy, "Design and analysis of hybrid PSO–GSA tuned PI and SMC controller for DC–DC Cuk converter," *IET Circuits Devices Syst.*, vol. 13, no. 3, pp. 374–384, 2019.
[41] G. S. Priya and P. Sivakumar, "Analysis of antlion optimizer-based ABT for automatic generation control of an interconnected power system," *Soft Comput.*, vol. 23, no. 18, pp. 8563–8577, Sep. 2019.

[42] S. R. Inkollu and V. R. Kota, "Optimal setting of FACTS devices for voltage stability improvement using PSO adaptive GSA hybrid algorithm," *Eng. Sci. Technol., Int. J.*, vol. 19, no. 3, pp. 1166–1176, Sep. 2016.
[43] V. Veerasamy, N. I. A. Wahab, R. Ramachandran, A. Vinayagam, M. L. Othman, H. Hizam, and J. Satheeshkumar, "Automatic load frequency control of a multi-area dynamic interconnected power system using a hybrid PSO-GSA-tuned PID controller," *Sustainability*, vol. 11, no. 24, p. 6908, 2019.
[44] M. Hasni, M. Boudour, N. E. L. Y. Kouba, and M. Menaa, "Optimal AGC scheme design using hybrid particle swarm optimisation and gravitational search algorithm," *Int. J. Power Energy Convers.*, vol. 10, no. 2, pp. 241–263, 2019.
[45] W. M. Spears and D. F. Spears, *Physicomimetics: Physics-Based Swarm Intelligence*, 1st ed. Berlin, Germany: Springer, 2012.
[46] D.-J. Lee and L. Wang, "Small-signal stability analysis of an autonomous hybrid renewable energy power generation/energy storage system part I: Time-domain simulations," *IEEE Trans. Energy Convers.*, vol. 23, no. 1, pp. 311–320, Mar. 2008.
[47] M. A. Johnson and M. H. Moradi, *PID Control: New Identification and Design Methods*. London, U.K.: Springer-Verlag, 2005.
[48] C. B. Vishwakarma and R. Prasad, "Time domain model order reduction using Hankel matrix approach," *J. Franklin Inst.*, vol. 351, no. 6, pp. 3445–3456, Jun. 2014.
[49] B. Lekshmi Sree and M. G. Umamaheswari, "A hankel matrix reduced order SEPIC model for simplified voltage control optimization and MPPT," *Sol. Energy*, vol. 170, pp. 280–292, Aug. 2018.

VEERAPANDIYAN VEERASAMY (Graduate Student Member, IEEE) received the bachelor's degree in electrical and electronics engineering from the Panimalar Engineering College, India, in 2013, and the M.E. degree in power systems engineering from the Government College of Technology, India, in 2015. He is currently pursuing the Ph.D. degree in power systems with University Putra Malaysia, Malaysia. Since 2015, he has been working as an Assistant Professor at the Department of Electrical and Electronics Engineering, Rajalakshmi Engineering College, India. His research areas include the design of robust controllers for power system application, fault classification, and power system monitoring.

NOOR IZZRI ABDUL WAHAB (Senior Member, IEEE) graduated in electrical and electronic engineering from The University of Manchester Institute of Science and Technology (UMIST), U.K., in 1998. He received the M.Sc. degree in electrical power engineering from University Putra Malaysia (UPM), in 2002, and the Ph.D. degree in electrical, electronic and system engineering from Universiti Kebangsaan Malaysia (UKM), in 2010. He is currently an Associate Professor with the Department of Electrical and Electronic Engineering, Faculty of Engineering, UPM. He has more than 100 publications under his name. He is a Researcher and the Founding Member of the Centre for Advanced Power and Energy Research (CAPER), UPM. His areas of interest include power system stability studies (dynamic and control), application of artificial intelligence in power systems, and power system quality. He is a member of The Institution of Engineers, Malaysia (IEM) and the Institution of Engineering and Technology, (IET), U.K. He is a Registered Chartered Engineer under the Engineering Council U.K., and IET U.K., and a Professional Engineer (Ir.) awarded by the Board of Engineers Malaysia (BEM).

RAJESWARI RAMACHANDRAN (Member, IEEE) received the bachelor's degree in electrical and electronics engineering and the master's degree in power systems engineering from the Thiagarajar College of Engineering, Madurai, India, in 1995 and 1998, respectively, and the Ph.D. degree from Anna University, Chennai, India, in 2009. She has been an Associate Professor with the Department of Electrical and Electronics Engineering, Government College of Technology, since 2009. Her research areas of interest include power system operation and control (dynamic and stability studies) and application of soft computing techniques to power systems.

MOHAMMAD LUTFI OTHMAN (Senior Member, IEEE) received the B.Sc. degree (Hons.) *(magna cum laude)* in electrical engineering from The University of Arizona (UofA), Tucson, AZ, USA, in 1990, and the M.Sc. and Ph.D. degrees in electrical power engineering from University Putra Malaysia (UPM), Seri Kembangan, Malaysia, in 2004 and 2011, respectively. He is currently an Associate Professor with the Department of Electrical and Electronics Engineering, Faculty of Engineering, UPM. He is a Researcher and the Founding Member of the Centre for Advanced Power and Energy Research (CAPER), UPM. His areas of research interest include, among others, numerical protective relay modeling, simulation, and operation analysis using computational-intelligent-based data mining and expert system approaches. His other researches involve energy efficiency management studies. He also practices as an electrical engineering consultant in electrical services installation works as an electrical director/partner in a local engineering consulting firm. He is a Professional Engineer (PEng) registered under the Board of Engineers Malaysia (BEM), a Chartered Engineer (CEng) registered under the Engineering Council U.K., a Registered Electrical Energy Manager (REEM) under Energy Commission Malaysia, a certified professional in measurement and verification (CPMV) under Malaysian Green Technology Corporation (under KETHHA), a Corporate Member of the Institution of Engineers Malaysia (IEM), a Senior Member of the IEEE Power and Energy Society (IEEE-PES) and the IEEE Computational Intelligence Society (IEEE-CIS), a member of the Institution of Engineering and Technology (IET) U.K., the International Rough Set Society (IRSS), the Asian Council of Science Editors (ACSE), the Academic Keys Who's Who in Engineering Higher Education (WWEHE), the International Rough Set Society (IRSS), a member of Phi Kappa Phi Honor Society, The University of Arizona, and a Graduate Technologist under the Malaysia Board of Technologist (MBOT). His biographical profile is mentioned in the Marquis Who's Who in the World 2016 (33rd Edition). As a professional engineer, he is a mentor and a professional interviewer for IEM/BEM Professional Engineer and the Engineering Council U.K. Chartered Engineer aspirants.

HASHIM HIZAM (Member, IEEE) received the B.Sc. and M.Sc. degrees in electrical and electronic engineering from Polytechnic University, Brooklyn, NY, USA, in 1993 and 1994, respectively, and the Ph.D. degree from Queen's University Belfast, Northern Ireland, in 2004. He joined UPM as a Lecturer, in 2004, where he is currently an Associate Professor with the Department of Electrical and Electronic Engineering, Faculty of Engineering. In UPM, he has served as the Head of the Electrical and Electronic Engineering Department, from 2006 to 2011, and the Deputy Dean for Academic, from March 2013 to June 2016. His research areas include power system analysis, protection, and renewable energy. He has published more than 80 journal articles and has successfully supervised several master's and Ph.D. students.

ANDREW XAVIER RAJ IRUDAYARAJ (Graduate Student Member, IEEE) received the bachelor's degree in electrical and electronics engineering from the J. J. College of Engineering and Technology, Tiruchirappalli, India, in 2012, and the M.E. degree in control and instrumentation engineering from the SRM Valliammai Engineering College, Chennai, India, in 2014. He is currently pursuing the Ph.D. degree in power systems with UPM, Malaysia. Since 2014, he has been working as an Assistant Professor at the Department of Electronics and Instrumentation Engineering, SRM Valliammai Engineering College. His research areas include the design of robust controllers for power system applications, system modeling, nonlinear controllers, and stability studies.

JOSEP M. GUERRERO (Fellow, IEEE) received the B.Sc. degree in telecommunications engineering, the M.Sc. degree in electronics engineering, and the Ph.D. degree in power electronics from the Polytechnic University of Catalonia, Barcelona, in 1997, 2000, and 2003, respectively. Since 2011, he has been a Full Professor with the Department of Energy Technology, Aalborg University, Denmark, where he is currently responsible for the Microgrid Research Program. He has also been the Chair Professor of Shandong University, since 2014, a Distinguished Guest Professor with Hunan University, since 2015, a Visiting Professor Fellow with Aston University, U.K., and a Guest Professor with the Nanjing University of Posts and Telecommunications, since 2016. In 2019, he became a Villum Investigator by The Villum Fonden, which supports the Center for Research on Microgrids (CROM), Aalborg University, where he is being the Founder and the Director. His research interests are oriented to different microgrid aspects, including power electronics, distributed energy-storage systems, hierarchical and cooperative control, energy management systems, smart metering and the Internet of Things for ac/dc microgrid clusters, and islanded minigrids. Specially focused on microgrid technologies applied to off shore wind and maritime microgrids for electrical ships, vessels, ferries, and seaports. He has published more than 500 journal articles in the fields of microgrids and renewable energy systems, which are cited more than 40 000 times. He received the Best Paper Award of the IEEE TRANSACTIONS ON ENERGY CONVERSION, from 2014 to 2015, the Best Paper Prize of IEEE-PES, in 2015, and the Best Paper Award of the *Journal of Power Electronics*, in 2016. During six consecutive years, from 2014 to 2019, he was awarded by the Clarivate Analytics (former Thomson Reuters) as a Highly Cited Researcher. In 2015, he was elevated as the IEEE Fellow for his contributions on distributed power systems and microgrids. He is an Associate Editor of several IEEE TRANSACTIONS.

JEEVITHA SATHEESH KUMAR received the bachelor's degree in electrical and electronics engineering from the College of Engineering, Chennai, India, in 2016, and the M.E. degree in power systems engineering from the Government College of Technology (GCT), Coimbatore, India, in 2018, where she is currently pursuing the Ph.D. degree in power systems. Since 2019, she has been working as an Assistant Professor at the Department of Electrical and Electronics Engineering, Tamilnadu College of Engineering, Coimbatore. Her research areas include the design of artificial intelligence-based controllers for power system applications and optimization techniques.